Bioorganic & Medicinal Chemistry Letters 22 (2012) 2681–2683

Contents lists available at SciVerse ScienceDirect

Bioorganic & Medicinal Chemistry Letters

journal homepage: www.elsevier.com/locate/bmcl

Double-stranded oligonucleotides containing 5-aminomethyl-2′-deoxyuridine form thermostable anti-parallel triplexes with single-stranded DNA or RNA

Aya Shibata [a], Yoshihito Ueno [b,*], Mari Iwata [a], Haruka Wakita [a], Akira Matsuda [c], Yukio Kitade [a]

[a] Department of Biomolecular Science, Faculty of Engineering, Gifu University, Yanagido, Gifu 501-1193, Japan
[b] Department of Applied Life Science, Faculty of Applied Biological Sciences, Gifu University, Yanagido, Gifu 501-1193, Japan
[c] Graduate School of Pharmaceutical Sciences, Hokkaido University, Kita-12, Nishi-6, Kita-ku, Sapporo 060-0812, Japan

ARTICLE INFO

Article history:
Available online 14 March 2012

Keywords:
DNA
RNA
Triplex
Antisense
Aminoalkyl linker
Thermal stability

ABSTRACT

This Letter describes the synthesis and properties of double-stranded antisense oligonucleotides connected with a pentaerythritol linker. We found that double-stranded antisense oligonucleotides with aminomethyl residues have high affinity for single-stranded DNA or RNA in buffer solutions with and without $MgCl_2$. Thus, these oligonucleotides would be useful as antisense oligonucleotides for targeting single-stranded RNA through triplex formation.

Thanks to the discovery of a large number of non-coding RNAs, gene suppression by using antisense oligonucleotides has once again attracted much attention.[1–3] An antisense oligonucleotide binds to the target mRNA via Watson–Crick hydrogen bonds, whereas an antigene oligonucleotide binds to the major groove of double-stranded DNA by Hoogsteen or reverse Hoogsteen hydrogen bonds and forms a local triple helix (triplex).[4] Recently, we reported an approach whereby single-stranded DNA or RNA is targeted through triplex formation by using a branched oligonucleotide.[5–7]

Approaches using branched oligonucleotides can be classified into 2 categories based on the orientation of the triplexes: one method utilizes parallel triplexes, in which the third strand binds to the second strand via Hoogsteen hydrogen bonds (Fig. 1a), whereas the other method utilizes antiparallel triplexes, where the third strand binds to the second strand via reverse Hoogsteen hydrogen bonds (Fig. 1b). In a previous report, we described the synthesis of double-stranded antisense oligonucleotides connected with a pentaerythritol linker that could target single-stranded DNA or RNA by forming parallel triplexes.[5–7] It was found that the double-stranded oligonucleotides formed more thermally stable triplexes than the corresponding Watson–Crick duplex with a single-stranded RNA.[6,7] This suggests that the double-stranded oligonucleotides are useful as an antisense oligonucleotide. In this Letter, we describe the synthesis and properties of double-stranded antisense oligonucleotides that can target single-stranded DNA or RNA by forming antiparallel triplexes.

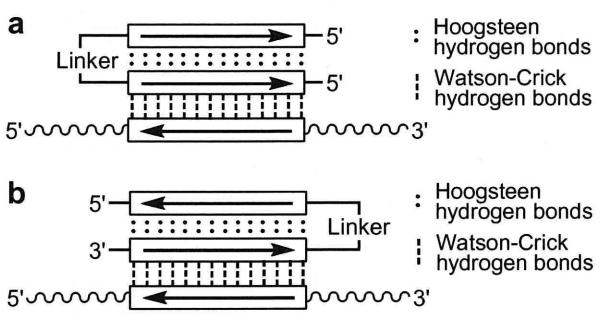

Figure 1. Schematic representation of branched oligonucleotides binding to single-stranded nucleic acids.

Thus far, oligonucleotide analogs carrying various polyamines have been synthesized,[8–14] and some of them have been shown to increase the thermal stability of duplexes and parallel triplexes. However, to the best of our knowledge, the stabilization effects of aminoalkyl modifications on antiparallel triplex formation have not been examined. X-ray crystal structure analysis of antiparallel triplexes showed that the 5-position of the thymidine residues of the third strand is positioned very close to the phosphate backbone

* Corresponding author. Tel./fax: +81 58 293 2919.
E-mail address: uenoy@gifu-u.ac.jp (Y. Ueno).

0960-894X/$ - see front matter © 2012 Elsevier Ltd. All rights reserved.
http://dx.doi.org/10.1016/j.bmcl.2012.03.024

target duplex

II 3'-d(GAGGAGGGAGGA)-5'

I 5'-d(CTCCTCCCTCCT)-3'

Z =

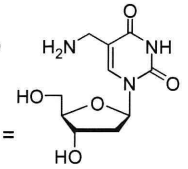

	3rd strand	K_d (nM)
III	5'-d(GTGGTGGGTGGT)-3'	115 ± 9
IV	5'-d(GTGGTGGGZGGT)-3'	128 ± 19
V	5'-d(GTGGZGGGZGGT)-3'	82 ± 4
VI	5'-d(GZGGZGGGZGGT)-3'	48 ± 6
VII	5'-d(GZGGZGGGZGGZ)-3'	68 ± 4

Figure 2. Binding abilities of the oligonucleotides for the target duplex.

of the second strand.[15] Thus, we hypothesized that introduction of an aminomethyl residue into the 5-position of the 2′-deoxyuridine in the third strand would increase the thermal stability of the antiparallel triplex because the ammonium cations of the aminomethyl residues would reduce the anionic electrostatic repulsion between the phosphate moieties.

Oligonucleotides containing 5-aminomethyl-2′-deoxyuridine (**Z**) were synthesized using the phosphoramidite method (Fig. 2). The synthetic route of a **Z** phosphoramidite is shown in Figure S1. All **Z**-containing oligonucleotides were synthesized using a DNA/RNA synthesizer. The obtained oligonucleotides were analyzed using matrix-assisted laser desorption/ionization time-of-flight mass spectrometry (MALDI-TOF/MS), and the observed molecular weights were in agreement with their structures.

First, binding of the aminomethyl-modified oligonucleotides to target DNA was examined using an electrophoretic mobility shift assay (EMSA). Figure 2 summarizes the dissociation constants (K_d) of the third strands bound to the duplex DNA target. The K_d of the unmodified third strand, **III**, to the target DNA was 115 ± 9 nM, whereas those of the third strands **V**, **VI**, and **VII** containing 2, 3, and 4 **Z** residues were 82 ± 4, 48 ± 6, and 68 ± 4 nM, respectively. Thus, this proved that the aminomethyl modification at the 5-position of the 2′-deoxyuridine in the third strand increases the stability of the antiparallel triplex. The K_d (128 ± 19 nM) of the third strand, **IV**, containing 1 **Z** residue was slightly lower than that of the unmodified third strand, **III**. Thus, plural **Z** residues seemed to be required for the triplex stabilization.

Branched oligonucleotides **IX** and **X** were synthesized using an appropriately protected pentaerythritol linker (Fig. 3). The stability of triplexes formed with these oligonucleotides was studied by thermal denaturation in Tris–HCl buffer solution (15 mM, pH 7.0) containing 25 mM NaCl and 5 mM $MgCl_2$ (Figs. 3 and S2). One transition was observed in the melting profile when branched oligonucleotide **IX** and single-stranded RNA **VIII** were used, and the melting temperature (T_m) was 67.6 °C. In contrast, the T_m of the duplex between single-stranded DNA **II** and RNA **VIII** was 54.5 °C. The increment in the absorbance melting curve of the **VIII**:**IX** complex was greater than that of the **VIII**:**II** duplex. This means that thermal denaturation from triplex to complete random coil for the **VIII**:**IX** complex occurred cooperatively in a single transition. On the other hand, the **VIII**:**II**:**III** triplex did not show a clear T_m transition, that might be due to aggregation of the oligonucleotide strands containing many guanine residues. Thus, it turned out that the oligonucleotide **IX** connected with the pentaerythritol linker forms a more thermostable triplex with the single-stranded RNA **VIII** than the corresponding **VIII**:**II** duplex. We also performed a thermal denaturation study with target RNA that contained one base mismatch (Fig. S3). The ΔT_m (T_m [a complex between an oligonucleotide and a complementary target] − T_m [a complex between an oligonucleotide and a target containing a mismatched base]) ranged from −7.2 to −12.4 °C. Thus, it was found that the branched oligonucleotide **IX** has sufficient base discrimination ability as an antisense oligonucleotide. Incorporation of 3 aminomethyl residues into the branched oligonucleotide slightly stabilized the triplex in the buffer solution containing $MgCl_2$. The ΔT_m between the triplexes **VIII**:**X** and **VIII**:**IX** was +2.7 °C. Similar phenomena were observed when single-stranded DNA **I** was used as the target (Fig. 3, top graph).

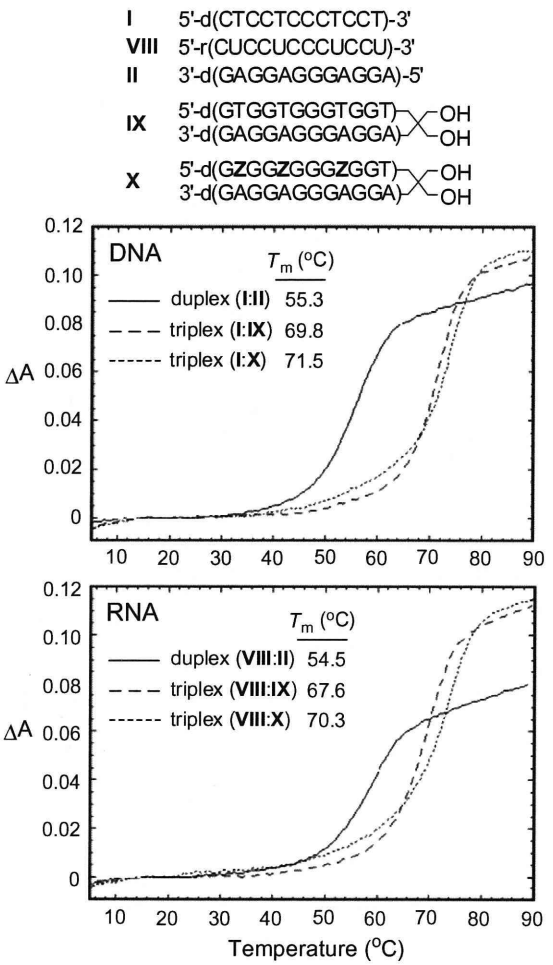

Figure 3. UV melting profiles. Melting experiments were performed in Tris–HCl buffer solution (15 mM, pH 7.0) containing 25 mM NaCl and 5.0 mM $MgCl_2$. The concentrations of the complexes were 2.0 μM.

It was reported that divalent cations, such as Mg^{2+}, are necessary for the formation of an antiparallel triplex.[16,17] Next, we demonstrated thermal denaturation in a buffer solution that did not contain $MgCl_2$. As shown in Fig. S2, the T_m of the complexes **I**:**IX**, **I**:**X**, **VIII**:**IX**, and **VIII**:**X** were significantly decreased. The T_m of the complexes were almost equal to those of the corresponding **I**:**II** and **VIII**:**II** duplexes. However, intriguingly, the increment in the absorbance melting curves of the **VIII**:**X** complex was greater than that of the **VIII**:**II** duplex. This suggested that the aminomethyl residue-containing branched oligonucleotide **X** formed an antiparallel triplex with the single-stranded RNA **VIII** in the absence of Mg^{2+}. The circular dichroism spectrum demonstrated not only triplex formation between the branched oligonucleotide **X** and the target RNA **VIII** but also triplex formation between the

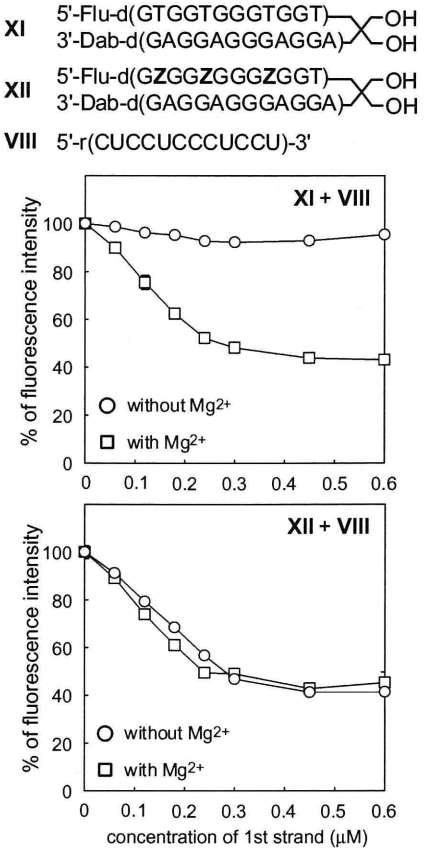

Figure 4. Profiles of the fluorescence intensities versus the first strand concentrations. Experiments were performed in Tris–HCl buffer solution (15 mM, pH 7.0) containing 25 mM NaCl in the presence or absence of 5.0 mM $MgCl_2$. The concentrations of the labeled oligonucleotides (**XI** and **XII**) were 0.30 μM. Excitation wavelength: 485 nm. Emission wavelength: 535 nm.

branched oligonucleotide **X** and the target DNA **I** in the absence of Mg^{2+} (Fig. S4).

In order to confirm the formation of the triplex, we next performed fluorescence resonance energy transfer (FRET) analysis. For this, we synthesized the branched oligonucleotides **XI** and **XII**, which were modified with fluorescein (Flu) at the 5′-end and with dabcyl (Dab) at the 3′-end as a quencher (Fig. 4). When the branched oligonucleotide **XI** was mixed with the target RNA **VIII** in the absence of Mg^{2+}, the fluorescence intensities of the solutions were almost the same irrespective of the concentrations of the first strand **VIII** (Fig. 4, top graph). On the other hand, the fluorescence intensities of the solutions decreased as the concentrations of the first strand **VIII** increased, and plateaued at a 1:1 branched oligonucleotide **XI** and first strand **VIII** ratio when the branched oligonucleotide **XI** was mixed with the target RNA **VIII** in the presence of Mg^{2+}. This indicates that the branched oligonucleotide **XI** forms a triplex with the target RNA **VIII** in the presence of Mg^{2+} but not in the absence of Mg^{2+}.

When the branched oligonucleotide **XII** containing the aminomethyl residues was used, the fluorescence intensities of the solutions decreased as the concentrations of the first strand **VIII** increased even in the absence of Mg^{2+}, and plateaued near a 1:1 branched oligonucleotide **XII** and first strand **VIII** ratio (Fig. 4, bottom graph). This proved that the branched oligonucleotide **XII**, which is modified with the aminomethyl residues, could form an antiparallel triplex even in the absence of a divalent cation such as Mg^{2+}.

In conclusion, we have demonstrated the synthesis of branched oligonucleotides containing aminomethyl residues, and found that these oligonucleotides have a high affinity for single-stranded DNA or RNA in buffer solutions with and without $MgCl_2$. Thus, these oligonucleotides would be useful as antisense oligonucleotides for targeting single-stranded RNA through triplex formation.

Acknowledgments

This study was supported in part by a Grant-in-Aid from the Koshiyama Research Grand and a Grant-in-Aid for Scientific Research (C) from the Japan Society for the Promotion of Science to Y.U.

Supplementary data

Supplementary data associated with this article can be found, in the online version, at http://dx.doi.org/10.1016/j.bmcl.2012.03.024.

References and notes

1. Carninci, P.; Kasukawa, T.; Katayama, S.; Gough, J.; Frith, M. C., et al *Science* **2005**, *309*, 1559.
2. Katayama, S.; Tomaru, Y.; Kasukawa, T.; Waki, K.; Nakanishi, M., et al *Science* **2005**, *309*, 1564.
3. Krützfeldt, J.; Rajewsky, N.; Braich, R.; Rajeev, K. G.; Tuschl, T.; Manoharan, M.; Stoffel, M. *Nature* **2005**, *438*, 685.
4. Thuong, N. T.; Hélène, C. *Angew. Chem., Int. Ed. Engl.* **1993**, *32*, 666.
5. Ueno, Y.; Takeba, M.; Mikawa, M.; Matsuda, A. *J. Org. Chem.* **1999**, *64*, 1211.
6. Ueno, Y.; Mikawa, M.; Hoshika, S.; Matsuda, A. *Bioconjugate Chem.* **2001**, *12*, 635.
7. Ueno, Y.; Shibata, A.; Matsuda, A.; Kitade, Y. *Bioconjugate Chem.* **2003**, *14*, 684.
8. Rajeev, K. G.; Jadhav, V. R.; Ganesh, K. N. *Nucleic Acids Res.* **1997**, *25*, 4187.
9. Cuenoud; Casset, F.; Hüsken, D.; Natt, F.; Wolf, R. M.; Altmann, K. H.; Martin, P.; Moser, H. E. *Angew. Chem., Int. Ed.* **1998**, *37*, 1288.
10. Bijapur, J.; Keppler, M. D.; Bergqvist, S.; Brown, T.; Fox, K. R. *Nucleic Acids Res.* **1999**, *27*, 1802.
11. Ueno, Y.; Tomino, K.; Sugimoto, I.; Matsuda, A. *Tetrahedron* **2000**, *56*, 7903.
12. Atsumi, N.; Ueno, Y.; Kanzaki, M.; Shuto, S.; Matsuda, A. *Bioorg. Med. Chem.* **2001**, *10*, 2933.
13. Puri, N.; Majumdar, A.; Cuenoud, B.; Natt, F.; Matin, P.; Boyd, A.; Miller, P. S.; Seidman, M. M. *Biochemistry* **2001**, *41*, 7716.
14. Brazier, J. A.; Shibata, T.; Townsley, J.; Taylor, B. F.; Frary, E.; Williams, N. H.; Williams, D. M. *Nucleic Acids Res.* **2005**, *33*, 1362.
15. Radhakrishnan, I.; Patel, D. J. *Structure* **1993**, *1*, 135.
16. Giovannangeli, C.; Rougée, M.; Garestier, T.; Thuong, N. T.; Hélène, C. *Proc. Natl. Acad. Sci. U.S.A.* **1992**, *89*, 8631.
17. Malkov, V. A.; Voloshin, O. N.; Soyfer, V. N.; Frank-Kamenetskii, M. D. *Nucleic Acids Res.* **1993**, *21*, 585.

Analytical Biochemistry 426 (2012) 129–133

Contents lists available at SciVerse ScienceDirect

Analytical Biochemistry

journal homepage: www.elsevier.com/locate/yabio

Improved identification of agonist-mediated $G\alpha_i$-specific human G-protein-coupled receptor signaling in yeast cells by flow cytometry

Jun Ishii [a], Miyuki Moriguchi [b], Kiyotaka Y. Hara [a], Seiji Shibasaki [c], Hideki Fukuda [b], Akihiko Kondo [b,*]

[a] Organization of Advanced Science and Technology, Kobe University, Nada, Kobe 657-8501, Japan
[b] Department of Chemical Science and Engineering, Graduate School of Engineering, Kobe University, Nada, Kobe 657-8501, Japan
[c] Department of Pharmacy, School of Pharmacy, Hyogo University of Health Sciences, Chuo, Kobe 650-8530, Japan

ARTICLE INFO

Article history:
Received 13 February 2012
Received in revised form 3 April 2012
Accepted 5 April 2012
Available online 11 April 2012

Keywords:
G-protein-coupled receptor
Yeast
Signaling assay
Flow cytometry

ABSTRACT

Flow cytometry enables comparative quantification, population analysis, and high-throughput screening of agonist-mediated G-protein-coupled receptor (GPCR) signaling in genetically engineered yeasts. By using flow cytometry, we found that transformation of yeast cells with a low plasmid number is critical both for the construction of large screening libraries and for stable signal transmission in cell ensembles. Based on these findings, we constructed an engineered yeast strain for the improved identification of signal promotion by $G\alpha_i$-specific human GPCRs using flow cytometry.

G-protein-coupled receptors (GPCRs)[1] regulate various physiological processes, including taste, smell, vision, heart rate, blood pressure, neurotransmission, and cell growth, by responding to external stimuli [1]. Therefore, GPCRs are widely studied as major molecular targets in drug discovery research [2]. GPCRs are cell surface 7-transmembrane receptors that transduce signals via heterotrimeric guanine nucleotide binding proteins (G-proteins) comprising Gα-, Gβ- and Gγ-subunits in all eukaryotes [3].

The eukaryotic unicellular yeast, *Saccharomyces cerevisiae*, is a typical host cell used to study GPCRs at the molecular level. Compared with mammalian cell lines, *S. cerevisiae* provides a simple and predictive way in which to study GPCR signaling because it expresses only one kind of G-protein [4–6]. In addition, *S. cerevisiae* offers a crucial advantage for the screening of functional residues [7,8] and ligand binding [9,10] due to its rapid proliferation and amenability to genetic manipulation compared with other eukaryotes.

In general, reporter genes such as *HIS3* (auxotrophy), *lacZ* (colorimetry), and *luc* (luminometry) are often used to detect the activation of signaling pathways by heterologously expressed GPCRs in yeast cells [7–11]. These reporter genes offer comprehensive screening, comparative quantification, and extremely high detection sensitivity, respectively. In contrast, we have developed a signal-responsive assay system using the green fluorescent protein (*GFP*) gene as the reporter (Fig. 1) [4–6,12–15]. This system is applicable to flow cytometry and, therefore, enables comparative quantification, population analysis, and quantitative high-throughput screening to be performed [16–19]. To date, we have engineered several yeast strains to express heterologous GPCRs that activate signaling pathways in response to agonist stimulation [4–6,12–15]. However, we have not compared the relative suitability of these strains for flow cytometry.

In the current study, therefore, we evaluated a selection of these engineered yeast strains by flow cytometry. The index parameters, active cell population (proportion of signal-activated cells to total cells) and average GFP intensity (or signal-to-noise (S/N) ratio), were analyzed by flow cytometry in 10,000 cells treated with agonists. Because transformation efficiency is an important factor for library construction, colony-forming unit efficiency was also determined by counting the number of colonies generated following transformation of yeast cells with plasmids encoding heterologous GPCRs.

Materials and methods

Media

Synthetic dextrose (SD) medium contained 6.7 g/L yeast nitrogen base without amino acids (YNB, BD Diagnostic Systems,

* Corresponding author. Fax: +81 78 803 6196.
E-mail address: akondo@kobe-u.ac.jp (A. Kondo).

[1] *Abbreviations used:* GPCR, G-protein-coupled receptor; G-protein, guanine nucleotide binding protein; GFP, green fluorescent protein; SD, synthetic dextrose; SC, synthetic complete; AP, alkaline phosphatase; SSTR5, somatostatin receptor subtype 5; 5-FOA, 5-fluoroorotic acid; S-14, somatostatin 14; Gi3tp, Gpa1/$G\alpha_{i3}$ transplant; S/N, signal-to-noise.

0003-2697/$ - see front matter © 2012 Elsevier Inc. All rights reserved.
http://dx.doi.org/10.1016/j.ab.2012.04.012

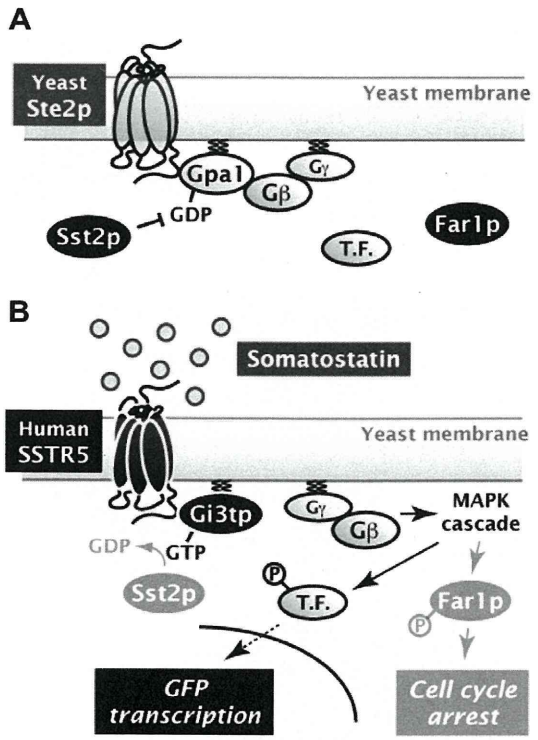

Fig.1. Outline of engineering strategy for SSTR5 signaling assay. (A) Schematic representation of major proteins involved in pheromone signal transduction in wild-type yeast. Yeast Ste2p, yeast endogenous GPCR; Gpa1, yeast endogenous Gα-subunit; Sst2p, Gpa1-specific GTPase-activating protein (a member of regulator of G-protein signaling (RGS) family that stimulates hydrolysis of GTP to GDP); Far1p, cyclin-dependent kinase inhibitor (mediates cell cycle arrest in response to pheromone signaling); T.F., transcription factor. (B) Schematic representation of engineered components of SSTR5 signaling assays. Yeast Ste2p was deleted to avoid competitive expression by the endogenous yeast GPCR. Alternatively, human SSTR5 was expressed from a multicopy episomal plasmid under the control of the constitutive *PGK1* promoter. A yeast–human chimeric G-protein in which the carboxyl-terminal 5 amino acid residues of Gpa1p were replaced by the equivalent residues to the human $G\alpha_{i3}$ (Gpa1/$G\alpha_{i3}$ transplant, Gi3tp) was substituted for Gpa1p. Sst2p was deleted to confer hypersensitivity to agonists. Far1p was deleted not only to promote cell cycle progression by avoiding G1 arrest even in signal-activated states but also to allow the recovery of episomal plasmids from signal-activated yeast cells, which is important for extensive screening. *GFP* reporter gene under the control of signal-responsive *FIG1* promoter was used to sense the SSTR5 signaling in the presence of somatostatin.

Sparks, MD, USA) and 20 g/L glucose. For SDM71 medium, 200 mM 3-(*N*-morpholino)-2-hydroxypropanesulfonic acid (Mopso, Nacalai Tesque, Kyoto, Japan) was added to SD medium to adjust the pH to 7.1. Amino acids and nucleotides (20 mg/L histidine, 60 mg/L leucine, 20 mg/L methionine, and 20 mg/L uracil) were supplemented into each medium to provide the relevant auxotrophic components. For synthetic complete (SC) medium, a variety of nutrients, including adenine, uracil, inositol, and *p*-aminobenzoic acid, as well as a complete range of amino acids were added into SD medium. To produce solid medium, 2% (w/v) agar was added when appropriate.

Plasmid constructions

All plasmids used in this study are listed in Table 1. All primers used for plasmid construction are listed in Supplementary Table 1 (see Supplementary material). A flow diagram for plasmid construction by the replacement of Gpa1p with Gi3tp is presented in Supplementary Fig. 1. DNA fragments corresponding to the respective upstream and downstream regions of the *GPA1* gene (*GPA5′* and *GPA3′*, 500 bp each) were amplified from BY4741 [20] genomic DNA and digested with *SacI–XhoI* and *XhoI–SphI*, respectively. The digested fragments were then simultaneously inserted into the *SacI–SphI* sites of pUC19 (Takara Bio, Shiga, Japan) by connecting the *XhoI* sites to generate the pI-GPA5.3 plasmid. A DNA fragment corresponding to the *URA3* selectable marker (containing 50 nt of the homologous region directly upstream of *GPA3′*, *hr50*) was amplified from pRS406 (American Type Culture Collection, Manassas, VA, USA) and digested with *XhoI* and *SalI*. The digested fragment was then inserted into the *XhoI* site of alkaline phosphatase (AP)-treated pI-GPA5.3 to retain the *XhoI* site at the *GPA5′* side, yielding the pUI-GPA5.3 plasmid. A DNA fragment encoding the *Gi3tp* gene (Gpa1/$G\alpha_{i3}$ transplant; the coding sequence for the carboxyl-terminal 5 amino acid residues of Gpa1p (KIGII) was replaced by the equivalent human $G\alpha_{i3}$ residues (ECGLY) [21]) was amplified from pSL-Gi3tp [4] and digested with *XhoI*. The digested fragment was then inserted into the *XhoI* site of AP-treated pUI-GPA5.3 to connect to the start codon of the *Gi3tp* gene at the *GPA5′* side, creating the pUI2-Gi3tp plasmid. A DNA fragment encoding the human somatostatin receptor subtype 5 (*SSTR5*) gene was amplified from pBlue-SSTR5-HA [5] and digested with *NheI–BglII*. The digested fragment was then inserted into the same sites of pGK421 [4,5], yielding the pGK421-SSTR5 plasmid.

Yeast strains

All yeast strains used in this study were generated from the BY4741 parental strain [20] and are listed in Table 1. A flow diagram for the construction of the yeast strain by substituting Gi3tp for Gpa1p is presented in Supplementary Fig. 2 (see Supplementary material). Transformation with linear DNA fragments was performed using the lithium acetate method [22]. The DNA fragment containing *GPA5′-Gi3tp-hr50-URA3-GPA3′* was prepared by digestion of pUI2-Gi3tp at the *SpeI* and *AseI* sites located in the *GPA5′* and *GPA3′* regions, respectively. The prepared linear DNA fragment was used to transform the IMFD-70 strain [5], and the transformant was selected on solid SD medium lacking uracil. After confirming integration of the DNA in the correct orientation, the cells were maintained on SC medium containing 1 mg/ml 5-fluoroorotic acid (5-FOA, Fluorochem, Derbyshire, UK) to eliminate the *URA3* selectable marker between the *hr50* and *GPA3′* genes by homologous recombination with counter selection. The strain substituted with the *Gi3tp* gene for the *GPA1* gene was designated as IMFD-72. Transformation with plasmids was also performed using the lithium acetate method to obtain all transformants used for assays.

SSTR5 signaling assay

To assay signal transduction mediated by the human SSTR5 receptor, the transformants were grown in SD medium at 30 °C. Cells were then inoculated into 50 ml of SDM71 medium to give an initial optical density of 0.03 at 600 nm (OD_{600} = 0.03). Cultures were grown at 30 °C with shaking at 150 rpm overnight and harvested. After washing, the cells were adjusted to an OD_{600} = 10 with sterile water. The cell suspensions (10 μl, to give a final OD_{600} = 1) and 100 or 0 μM somatostatin 14 (S-14, Calbiochem/Merck4Biosciences, Darmstadt, Germany) (10 μl, to give a final concentration of 10 or 0 μM) were added into the wells of 96-well cluster dishes containing the fresh SDM71 medium (80 μl), and then the plates were incubated at 30 °C with shaking at 150 rpm for 4 h. The total cell suspension volumes (100 μl) were directly diluted into test tubes containing sheath solution, and GFP fluorescence was measured using a BD FACSCalibur flow cytometer (BD Biosciences, San Jose, CA, USA). The green fluorescence signal of 10,000 cells was excited with a 488-nm argon laser and collected

Table 1
Yeast strains and plasmids used in this study.

Strain or plasmid	Specific features
Yeast strains	
BY4741	*MATa his3Δ1 leu2Δ0 met15Δ0 ura3Δ0*
MI-150	BY4741 *gpa1Δ::kanMX4 sst2Δ ste2Δ*
IM-50	BY4741 *sst2Δ::AUR1-C ste2Δ::LEU2*
IMF-50	BY4741 *sst2Δ::AUR1-C ste2Δ::LEU2 fig1Δ::EGFP*
IMFD-50	BY4741 *sst2Δ::AUR1-C ste2Δ::LEU2 fig1Δ::EGFP his3Δ::P_{FIG1}-EGFP*
IMFD-70	BY4741 *sst2Δ::AUR1-C ste2Δ::LEU2 fig1Δ::EGFP his3Δ::P_{FIG1}-EGFP far1Δ*
IMFD-72	BY4741 *sst2Δ::AUR1-C ste2Δ::LEU2 fig1Δ::EGFP his3Δ::P_{FIG1}-EGFP far1Δ gpa1Δ::Gi3tp*
Plasmids	
pUC19	Cloning vector
pI-GPA5.3	*GPA5′-GPA3′* in pUC19
pUI-GPA5.3	*GPA5′-hr50-URA3-GPA3′* in pUC19
pUI2-Gi3tp	*GPA5′-Gi3tp-hr50-URA3-GPA3′* in pUC19
pGK421	Expression vector containing *PGK1* promoter, 2μ origin and *MET15* marker
pGK421-SSTR5	Human SSTR5 receptor expression, *PGK1* promoter, 2μ origin and *MET15* marker
pSL-Gi3tp	Yeast–human chimeric Gα (Gi3tp) expression, *GPA1* promoter, *CEN/ARS* origin and *LEU2* marker
pSL-GPA1	Yeast endogenous Gα (Gpa1p) expression, *GPA1* promoter, *CEN/ARS* origin and *LEU2* marker
pMHG-FIG1	*GFP* reporter gene expression, *FIG1* promoter, 2μ origin and *HIS3* marker

through a 530/30-nm bandpass (FL1) filter. The data were analyzed using FlowJo software (version 8.5.3, Tree Star, Ashland, OR, USA).

Measurement of colony-forming unit efficiency

Cells were transformed with 1 μl of each plasmid (1 μg/μl) and selected on appropriate SD selectable solid medium at 30 °C for 2 to 4 days. Transformation of plasmids was performed using the lithium acetate method. Colony-forming units were determined from the numbers of colonies generated on the SD selectable solid medium.

Results and discussion

To compare the strains by flow cytometry, human SSTR5, which endogenously signals via $G\alpha_i$ [23], was selected as a model for heterologous GPCRs expressed in engineered yeast cells. The natural peptide ligand, S-14 [24], was used as the agonist. In all engineered yeast strains, the *ste2Δ* allele was conferred to avoid the competitive expression of the endogenous yeast GPCR (Ste2p) (Fig. 1). The human SSTR5 receptor was expressed via a multicopy episomal plasmid under the control of constitutive *PGK1* promoter (pGK421-SSTR5) (Table 1).

Whereas the human SSTR5 receptor is known to transduce signals in yeast cells through the endogenous yeast Gα-subunit (Gpa1p) [4–6,21], the yeast–human chimeric G-protein, in which the carboxyl-terminal 5 amino acid residues of Gpa1p are replaced by the equivalent residues from human $G\alpha_{i3}$ ($Gpa1/G\alpha_{i3}$ transplant, Gi3tp) (Fig. 1), has been shown to improve signal transmission via $G\alpha_i$-specific SSTR5 in yeast [21]. We previously constructed single-copy episomal plasmids that expressed the yeast–human chimeric Gi3tp or the yeast wild-type Gpa1p under the control of *GPA1* promoter (pSL-Gi3tp and pSL-GPA1) and a yeast strain (MI-150) with *gpa1Δ sst2Δ ste2Δ* triple deletion alleles [4] (Table 1). The *gpa1Δ* allele excluded signal transmission through the intrinsic yeast Gα-subunit, and the *sst2Δ* allele conferred hypersensitivity toward agonists by diminishing the activity of Gpa1-specific GTPase-activating protein [3,4] (Fig. 1). In addition, we also previously constructed a multicopy episomal plasmid (pMHG-FIG1) to express the *GFP* reporter gene under the control of the signal-responsive *FIG1* promoter [4] (Table 1).

First, we confirmed signal transduction by the MI-150 yeast strains transformed with pGK421-SSTR5, pSL-Gi3tp (or pSL-GPA1), and pMHG-FIG1 using a BD FACSCalibur flow cytometer and FlowJo software. We observed that S-14 mediated signal transduction via Gi3tp in the triple transformants by an increase in the active cell population compared with control cells (36.42–48.99%) (Fig. 2A and B). Next, we introduced pGK421-SSTR5 and pMHG-FIG1 into the yeast strain harboring *sst2Δ ste2Δ* double deletion alleles (IM-50) that expressed endogenous Gpa1p [14] (Table 1). Compared with the MI-150 triple transformant, this double transformant improved the active cell population (36.42–74.69%) that responded to S-14 (Fig. 2A and C). This observation was also supported by the increased average GFP intensity (signal-to-noise (S/N) ratio) in 10,000 cells (Fig. 3A and C). These

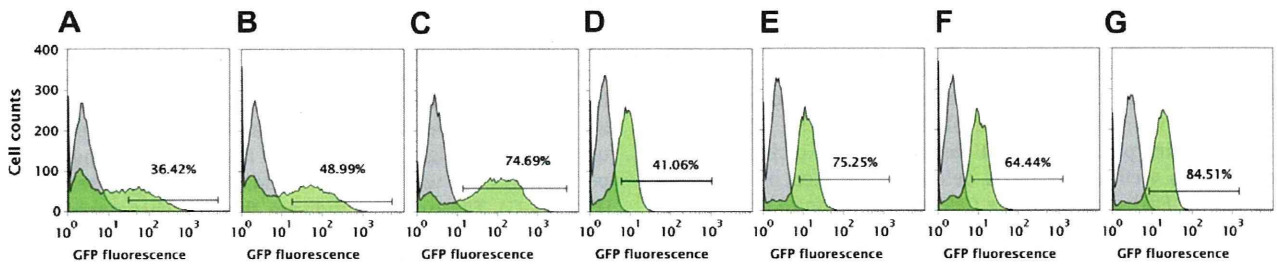

Fig.2. Active cell populations. Signal transduction in SSTR-expressing yeast cells was invoked with 10 μM S-14 and analyzed by a flow cytometer as described in Materials and Methods: (A) MI-150/pGK421-SSTR5/pSL-GPA1/pMHG-FIG1; (B) MI-150/pGK421-SSTR5/pSL-Gi3tp/pMHG-FIG1; (C) IM-50/pGK421-SSTR5/pMHG-FIG1; (D) IMF-50/pGK421-SSTR5; (E) IMFD-50/pGK421-SSTR5; (F) IMFD-70/pGK421-SSTR5; (G) IMFD-72/pGK421-SSTR5. Filled green and gray histograms represent the yeast cells incubated in pH-adjusted medium with and without S-14, respectively. Active cell populations were defined as the cell populations included in the areas where the populations of signal-unpromoted cells in the absence of S-14 were less than 0.1%. (For interpretation of the references to color in this figure legend, the reader is referred to the Web version of this article.)

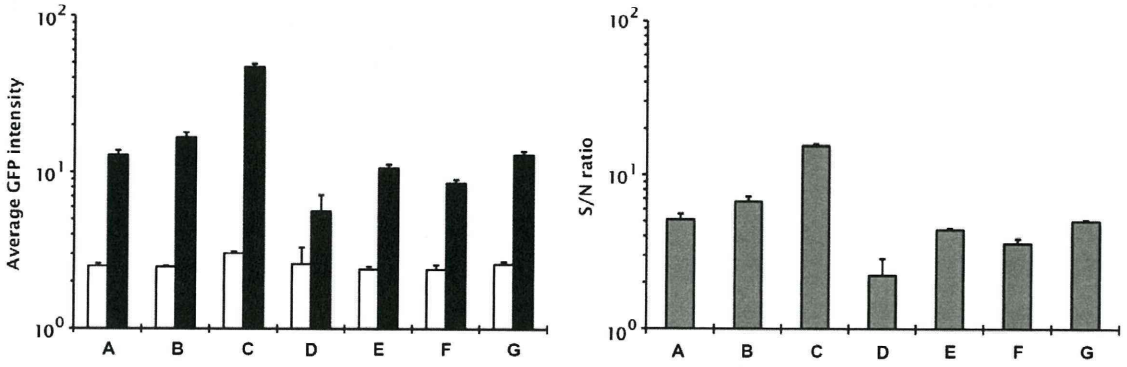

Fig.3. Average GFP intensities (left) and S/N ratios (right). Signal transduction in SSTR5-expressing yeast cells was invoked with 10 μM S-14 and analyzed by a flow cytometer as described in Materials and Methods: (A) MI-150/pGK421-SSTR5/pSL-GPA1/pMHG-FIG1; (B) MI-150/pGK421-SSTR5/pSL-Gi3tp/pMHG-FIG1; (C) IM-50/pGK421-SSTR5/pMHG-FIG1; (D) IMF-50/pGK421-SSTR5; (E) IMFD-50/pGK421-SSTR5; (F) IMFD-70/pGK421-SSTR5; (G) IMFD-72/pGK421-SSTR5. Black and white bars present the average GFP intensities of the yeast cells incubated in pH-adjusted medium with and without S-14, respectively. Gray bars present the S/N ratios. Error bars represent the standard deviations ($n = 3$).

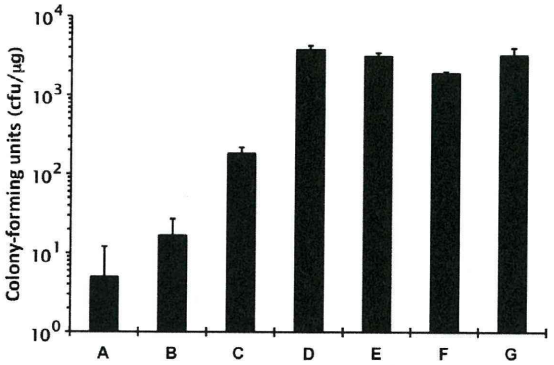

Fig.4. Colony-forming units obtained by transformation of yeast cells. Cells were transformed with 1 μl of each plasmid (1 μg/μl) as described in Materials and Methods: (A) MI-150/pGK421-SSTR5/pSL-GPA1/pMHG-FIG1; (B) MI-150/pGK421-SSTR5/pSL-Gi3tp/pMHG-FIG1; (C) IM-50/pGK421-SSTR5/pMHG-FIG1; (D) IMF-50/pGK421-SSTR5; (E) IMFD-50/pGK421-SSTR5; (F) IMFD-70/pGK421-SSTR5; (G) IMFD-72/pGK421-SSTR5. Colony-forming units were determined as the numbers of observed colonies on the appropriate selectable medium. Error bars represent the standard deviations ($n = 3$).

results suggest that recombinant protein expression by several plasmids attenuates the phenotypic stability of the yeast strains. Moreover, the IM-50 double transformant showed a higher score in the colony-forming unit assay than the MI-150 triple transformant (Fig. 4A–C), indicating that the transformation of yeast cells with a lower plasmid number is more efficient. Therefore, transformation with less than three plasmids may be more suitable for construction of the large libraries required to screen candidate receptor mutants and ligand substitutes.

Because of the results of the colony-forming unit assays from yeast strains transformed with two or three plasmids, we subsequently tested the engineered yeast strains that mediate signal transduction via one introduced plasmid only. The IMF-50 and IMFD-50 strains possess identical deletion alleles, including *sst2*Δ and *ste2*Δ as well as the *fig1*Δ deletion generated by replacing the genomic *FIG1* gene with the *GFP* reporter gene to enable agonist-mediated signal transduction to be detected by the appearance of green fluorescence [5] (Table 1). However, the IMFD-50 strain has an apparent difference with the IMF-50 strain conferred by an additional cassette that expresses the *GFP* reporter gene under the control of the signal-responsive *FIG1* promoter inserted into the function-deficient *HIS3* (*his3Δ1*) genomic locus [5] (Table 1). Compared with the strains harboring two or three plasmids, the IMF-50 strain harboring pGK421-SSTR5 exhibited a lower active cell population (41.06%) and a lower average GFP intensity (S/N ratio) following stimulation by S-14 (Figs. 2D and 3D). However, the colony-forming unit score of the IMF-50 strain was substantially augmented (Fig. 4D). In the presence of S-14, the IMFD-50 strain harboring pGK421-SSTR5 displayed higher values for active cell population (75.25%) and average GFP intensity (S/N ratio) than the IMF-50 strain harboring pGK421-SSTR5 as well as an elevated colony-forming unit score (Figs. 2E, 3E, and 4E). These results indicate that the two *FIG1* promoter-driven *GFP* reporter gene cassettes integrated into the chromosomes of the IMFD-50 strain enhance the green fluorescence signal in response to GPCR-mediated signal transduction.

Next, we evaluated the IMFD-70 strain (derived from the IMFD-50), which harbors a deletion in the *FAR1* gene that encodes a cyclin-dependent kinase inhibitor and mediates cell cycle arrest in response to receptor activation [3,5] (Table 1). Whereas the *far1*Δ allele promotes cell cycle progression by avoiding G1 arrest even in signal-activated states (Fig. 1), it also allows the recovery of episomal plasmids from signal-activated yeast cells that is important for extensive screening [14]. The IMFD-70 strain harboring pGK421-SSTR5 exhibited similar characteristics to the *FAR1*-intact IMFD-50 strain harboring pGK421-SSTR5 (Figs. 2F, 3F, and 4F), although the active cell population that responded to S-14 was slightly decreased by the *FAR1* deletion (64.44%) (Fig. 2F). Therefore, we attempted to elevate the active cell population while maintaining the colony-forming unit efficiency.

We constructed a new strain that expressed the yeast–human chimeric Gi3tp in place of yeast endogenous Gpa1p under the control of the genomic *GPA1* locus. Using the IMFD-70 strain, the gene encoding Gi3tp was substituted for the chromosomal *GPA1* gene by homologous recombination via the marker recycling method [25] to create the IMFD-72 yeast strain (Table 1 and Fig. 1). As expected from the results with episomal plasmids (Fig. 2A and B), the IMFD-72 strain harboring pGK421-SSTR5 substantially improved the active cell population while maintaining the colony-forming unit efficiency (Figs. 2G and 4G). It is notable that the active cell population value was the highest (84.51%) among all tested strains (Fig. 2A–G). These results indicate that the chromosomally integrated yeast–human chimeric *Gi3tp* gene contributed to the coupling of the $G\alpha_i$-specific human SSTR5 receptor. In addition, the lower number of plasmids in the IMFD-72 transformant also enabled stable signal transduction in the cell population and improved the colony-forming unit efficiency. Because the stable signal transduction (active cell population) and the colony-forming unit are more critical for the screening with flow cytometric

separation rather than the average GFP intensity (S/N ratio), the IMFD-72 yeast strain would be able to identify the $G\alpha_i$-specific receptor mutants and the ligand substitutes.

Conclusion

We used flow cytometry to evaluate the ability of previously constructed yeast strains to sense agonist-mediated signal transduction by genetically expressed human SSTR5. As a result, we found that reducing the number of plasmids introduced into the engineered yeast cells was a critical factor not only for the construction of the large library required for screening but also for enabling stable transmission of the signal in the cell ensembles. Based on these findings, we constructed the engineered IMFD-72 yeast strain by chromosomal integration of the yeast–human chimeric *Gi3tp* gene as a substitute for the *GPA1* gene and two cassettes of the signal-responsive *GFP* reporter gene in addition to the *far1*Δ *gpa1*Δ *sst2*Δ and *ste2*Δ deletion alleles. This IMFD-72 strain enabled improved flow cytometric separation to identify signal transduction mediated by the $G\alpha_i$-specific human SSTR5 GPCR. Because the impact of the yeast–human chimeric Gi3tp G-protein has been demonstrated for a variety of $G\alpha_i$-specific human GPCRs [21], the IMFD-72 strain should be applicable for the screening of human $G\alpha_i$-specific receptors other than SSTR5.

Acknowledgments

This work was supported mainly by a Grant-in-Aid for Scientific Research on Priority Areas (Life Surveyor) from the Ministry of Education, Culture, Sports, Science, and Technology (MEXT). It was also funded in part by the Special Coordination Funds for Promoting Science and Technology, Creation of Innovation Centers for Advanced Interdisciplinary Research Areas (Innovative Bioproduction Kobe, iBioK) from the MEXT of Japan, and AS ONE Corporation.

Appendix A. Supplementary data

Supplementary data associated with this article can be found, in the online version, at http://dx.doi.org/10.1016/j.ab.2012.04.012.

References

[1] O. Vögler, J.M. Barceló, C. Ribas, P.V. Escribá, Membrane interactions of G proteins and other related proteins, Biochim. Biophys. Acta 1778 (2008) 1640–1652.
[2] R. Heilker, M. Wolff, C.S. Tautermann, M. Bieler, G-protein-coupled receptor-focused drug discovery using a target class platform approach, Drug Discov. Today 14 (2009) 231–240.
[3] J. Ishii, N. Fukuda, T. Tanaka, C. Ogino, A. Kondo, Protein–protein interactions and selection: yeast-based approaches that exploit guanine nucleotide-binding protein signaling, FEBS J. 277 (2010) 1982–1995.
[4] Y. Iguchi, J. Ishii, H. Nakayama, A. Ishikura, K. Izawa, T. Tanaka, C. Ogino, A. Kondo, Control of signalling properties of human somatostatin receptor subtype-5 by additional signal sequences on its amino-terminus in yeast, J. Biochem. 147 (2010) 875–884.
[5] S. Togawa, J. Ishii, A. Ishikura, T. Tanaka, C. Ogino, A. Kondo, Importance of asparagine residues at positions 13 and 26 on the amino-terminal domain of human somatostatin receptor subtype-5 in signaling, J. Biochem. 147 (2010) 867–873.
[6] N. Fukuda, J. Ishii, M. Kaishima, A. Kondo, Amplification of agonist stimulation of human G-protein-coupled receptor signaling in yeast, Anal. Biochem. 417 (2011) 182–187.
[7] B. Li, M. Scarselli, C.D. Knudsen, S.K. Kim, K.A. Jacobson, S.M. McMillin, J. Wess, Rapid identification of functionally critical amino acids in a G protein-coupled receptor, Nat. Methods 4 (2007) 169–174.
[8] T.J. Baranski, P. Herzmark, O. Lichtarge, B.O. Gerber, J. Trueheart, E.C. Meng, T. Iiri, S.P. Sheikh, H.R. Bourne, C5a receptor activation: genetic identification of critical residues in four transmembrane helices, J. Biol. Chem. 274 (1999) 15757–15765.
[9] C. Klein, J.I. Paul, K. Sauvé, M.M. Schmidt, L. Arcangeli, J. Ransom, J. Trueheart, J.P. Manfredi, J.R. Broach, A.J. Murphy, Identification of surrogate agonists for the human FPRL-1 receptor by autocrine selection in yeast, Nat. Biotechnol. 16 (1998) 1334–1337.
[10] J.P. Manfredi, C. Klein, J.J. Herrero, D.R. Byrd, J. Trueheart, W.T. Wiesler, D.M. Fowlkes, J.R. Broach, Yeast α mating factor structure–activity relationship derived from genetically selected peptide agonists and antagonists of Ste2p, Mol. Cell. Biol. 16 (1996) 4700–4709.
[11] Y. Fukutani, T. Nakamura, M. Yorozu, J. Ishii, A. Kondo, M. Yohda, The N-terminal replacement of an olfactory receptor for the development of a yeast-based biomimetic odor sensor, Biotechnol. Bioeng. 109 (2012) 205–212.
[12] J. Ishii, N. Yoshimoto, K. Tatematsu, S. Kuroda, C. Ogino, H. Fukuda, A. Kondo, Cell wall trapping of autocrine peptides for human G-protein-coupled receptors on the yeast cell surface, in press.
[13] S. Ryo, J. Ishii, Y. Iguchi, N. Fukuda, A. Kondo, Transplantation of the GAL regulon into G-protein signaling circuitry in yeast, Anal. Biochem. 424 (2012) 27–31.
[14] J. Ishii, T. Tanaka, S. Matsumura, K. Tatematsu, S. Kuroda, C. Ogino, H. Fukuda, A. Kondo, Yeast-based fluorescence reporter assay of G protein-coupled receptor signalling for flow cytometric screening: *FAR1*-disruption recovers loss of episomal plasmid caused by signalling in yeast, J. Biochem. 143 (2008) 667–674.
[15] J. Ishii, S. Matsumura, S. Kimura, K. Tatematsu, S. Kuroda, H. Fukuda, A. Kondo, Quantitative and dynamic analyses of G protein-coupled receptor signaling in yeast using Fus1, enhanced green fluorescence protein (EGFP), and His3 fusion protein, Biotechnol. Prog. 22 (2006) 954–960.
[16] S. Müller, G. Nebe-von-Caron, Functional single-cell analyses: flow cytometry and cell sorting of microbial populations and communities, FEMS Microbiol. Rev. 34 (2010) 554–587.
[17] J. Ishii, K. Izawa, S. Matsumura, K. Wakamura, T. Tanino, T. Tanaka, C. Ogino, H. Fukuda, A. Kondo, A simple and immediate method for simultaneously evaluating expression level and plasmid maintenance in yeast, J. Biochem. 145 (2009) 701–708.
[18] N. Fukuda, J. Ishii, S. Shibasaki, M. Ueda, H. Fukuda, A. Kondo, High-efficiency recovery of target cells using improved yeast display system for detection of protein–protein interactions, Appl. Microbiol. Biotechnol. 76 (2007) 151–158.
[19] S. Shibasaki, A. Kawabata, J. Ishii, S. Yagi, T. Kadonosono, M. Kato, N. Fukuda, A. Kondo, M. Ueda, Construction of a novel synergistic system for production and recovery of secreted recombinant proteins by the cell surface engineering, Appl. Microbiol. Biotechnol. 75 (2007) 821–828.
[20] C.B. Brachmann, A. Davies, G.J. Cost, E. Caputo, J. Li, P. Hieter, J.D. Boeke, Designer deletion strains derived from *Saccharomyces cerevisiae* S288C: a useful set of strains and plasmids for PCR-mediated gene disruption and other applications, Yeast 14 (1998) 115–132.
[21] A.J. Brown, S.L. Dyos, M.S. Whiteway, J.H. White, M.A. Watson, M. Marzioch, J.J. Clare, D.J. Cousens, C. Paddon, C. Plumpton, M.A. Romanos, S.J. Dowell, Functional coupling of mammalian receptors to the yeast mating pathway using novel yeast/mammalian G protein α-subunit chimeras, Yeast 16 (2000) 11–22.
[22] D. Gietz, A. St Jean, R.A. Woods, R.H. Schiestl, Improved method for high efficiency transformation of intact yeast cells, Nucleic Acids Res. 20 (1992) 1425.
[23] L.N. Møller, C.E. Stidsen, B. Hartmann, J.J. Holst, Somatostatin receptors, Biochim. Biophys. Acta 1616 (2003) 1–84.
[24] R. Burgus, N. Ling, M. Butcher, R. Guillemin, Primary structure of somatostatin, a hypothalamic peptide that inhibits the secretion of pituitary growth hormone, Proc. Natl. Acad. Sci. USA 70 (1973) 684–688.
[25] R. Akada, T. Kitagawa, S. Kaneko, D. Toyonaga, S. Ito, Y. Kakihara, H. Hoshida, S. Morimura, A. Kondo, K. Kida, PCR-mediated seamless gene deletion and marker recycling in *Saccharomyces cerevisiae*, Yeast 23 (2006) 399–405.

Translational inhibition by deadenylation-independent mechanisms is central to microRNA-mediated silencing in zebrafish

Yuichiro Mishima[a,1], Akira Fukao[b,2], Tomoyoshi Kishimoto[a,2], Hiroshi Sakamoto[a], Toshinobu Fujiwara[b], and Kunio Inoue[a,1]

[a]Department of Biology, Graduate School of Science, Kobe University, 1-1 Rokkodaicho Nadaku, Kobe, Hyogo 657-8501, Japan; and [b]Institute of Microbial Chemistry, 3-14-23 Kamiosaki, Shinagawa-ku, Tokyo 141-0021, Japan

Edited by Joan A. Steitz, Howard Hughes Medical Institute, New Haven, CT, and approved December 5, 2011 (received for review August 15, 2011)

MicroRNA (miRNA) is a class of small noncoding RNA approximately 22 nt in length. Animal miRNA silences complementary mRNAs via translational inhibition, deadenylation, and mRNA degradation. However, the underlying molecular mechanisms remain unclear. A key question is whether these three outputs are independently induced by miRNA through distinct mechanisms or sequentially induced within a single molecular pathway. Here, we successfully dissected these intricate outputs of miRNA-mediated repression using zebrafish embryos as a model system. Our results indicate that translational inhibition and deadenylation are independent outputs mediated by distinct domains of TNRC6A, which is an effector protein in the miRNA pathway. Translational inhibition by TNRC6A is divided into two mechanisms: PAM2 motif-mediated interference of poly(A)-binding protein (PABP), and inhibition of 5′ cap- and poly(A) tail-independent step(s) by a previously undescribed P-GL motif. Consistent with these observations, we show that, in zebrafish embryos, miRNA inhibits translation of the target mRNA in a deadenylation- and PABP-independent manner at early time points. These results indicate that miRNA exerts multiple posttranscriptional outputs via physically and functionally independent mechanisms and that direct translational inhibition is central to miRNA-mediated repression.

MicroRNA (miRNA) is a class of small noncoding RNA approximately 22 nt in length. Previous studies have shown that miRNA plays a wide variety of regulatory roles in animals and plants (1). Animal miRNA silences partially complementary mRNAs (2). However, the mechanism of its action is under intense debate. Biochemical studies have shown a significant repression of miRNA target genes via translational inhibition (3). In contrast, transcriptome analyses of miRNA target genes have revealed that miRNA promotes mRNA degradation (4, 5). Genome-wide studies that analyzed mRNA stability and translation status in parallel have reached different conclusions concerning the relative contributions of these two outputs (6–8). In addition to these outputs, miRNA induces deadenylation of its target mRNA (5, 9, 10). Given that the translation status, poly(A) tail length and mRNA stability are closely linked to each other, whether these three outputs are independently induced by miRNA through distinct mechanisms or rather sequentially induced within single molecular pathway remains unknown (3, 11).

miRNA forms a complex with protein factors, called miRNA induced silencing complex (miRISC), to induce target mRNA silencing. Argonaute (Ago) protein is an integral component of miRISC and directly interacts with miRNA to support the binding of miRNAs to their target mRNAs (12). In addition to Ago, animal miRNA requires another miRISC component, TNRC6/GW182 (hereafter referred to as TNRC6), for target mRNA silencing (13). TNRC6 associates with the Ago-miRNA complex via multiple Ago-binding motifs in its N-terminal region (14, 15). In contrast, the C-terminal regions of TNRC6 have been identified as a silencing domain because this domain is sufficient to elicit posttranscriptional silencing (16, 17). Recent studies have shown that the silencing domains of TNRC6 bind to poly(A) binding protein (PABP). In the case of mammalian TNRC6, the interaction occurs mainly through direct interaction between the conserved sequence PAM2 (PABP-interacting motif 2), which is located at the anterior portion of the silencing domain, and the C-terminal MLLE domain of PABP (18–20). The TNRC6-PABP interaction accelerates deadenylation by CAF1/CCR4 in Krebs cell extract (18, 19). In human and fly cultured cells, the TNRC6-PABP interaction is required to support maximum repression by miRNA (20). These observations have led to a model proposing that, via TNRC6-PABP interactions, miRISC interferes with translation at the initiation step and/or induces mRNA deadenylation/degradation by increasing the susceptibility of the poly(A) tail to deadenylases (11, 18). However, this model does not address the hierarchy of multiple outputs induced by miRNA. In addition, the contribution of the TNRC6-PABP interaction in the miRNA pathway awaits further validation because poly(A) tail-independent repression by miRNA has been reported in several experimental systems (10, 21).

In the current study, we successfully dissected intricate outputs of miRNA-mediated repression using zebrafish embryos as a model system. Our results indicate that translational inhibition and deadenylation are independent outputs mediated by distinct domains of TNRC6A. Translational inhibition by TNRC6A is divided into two mechanisms: PAM2 motif-mediated interference of poly(A)-binding protein (PABP), and inhibition of 5′ cap- and poly(A) tail-independent step(s) by a previously undescribed P-GL motif. Consistent with these observations, we show that, in zebrafish embryos, miRNA inhibits translation of the target mRNA in a deadenylation- and PABP-independent manner at early time points.

Results

TNRC6A Induces Translational Inhibition and Deadenylation Through the Mid Domain in Zebrafish Embryos. To elucidate the mechanisms of miRNA-mediated repression, we investigated the repression activities of TNRC6 using zebrafish as an in vivo model system. As in other vertebrates, the genome of zebrafish encodes all three TNRC6 paralogues (TNRC6A, B and C) and additional TNRC6B and TNRC6C genes due to genome duplication. We focused on a unique zebrafish orthologue of TNRC6A in this study because all TNRC6 paralogues have a repressive activity in humans (17, 22). Zebrafish TNRC6A contains all of the conserved motifs/domains that were found in other TNRC6 ortholo-

Author contributions: Y.M. and K.I. designed research; Y.M., A.F., T.K., H.S., and T.F. performed research; Y.M., T.F., and K.I. analyzed data; and Y.M. and K.I. wrote the paper.

The authors declare no conflict of interest.

This article is a PNAS Direct Submission.

[1]To whom correspondence may be addressed. E-mail: yuichiro.mishima@people.kobe-u.ac.jp or kunio@kobe-u.ac.jp.

[2]A.F. and T.K. contributed equally to this work.

This article contains supporting information online at www.pnas.org/lookup/suppl/doi:10.1073/pnas.1113350109/-/DCSupplemental.

gues (13) (Fig. 1*A*). To identify the functional domain(s) in zebrafish TNRC6A that were responsible for silencing effects, we generated a series of deletion constructs and tested their effects in a λN-BoxB tethering assay in zebrafish embryos (Fig. 1 *A* and *B*). Tethering of full-length TNRC6A to Rluc-BoxB-poly(A) mRNA repressed Rluc activity to approximately 40% compared to the control construct encoding the HA-tagged N-peptide (HA-N) (Fig. 1*C*, full). As reported with other TNRC6 orthologues (16, 17), the silencing domain (SD) of zebrafish TNRC6A was sufficient to induce repression (Fig. 1*C*, SD). Furthermore, we found that the anterior half of the silencing domain (before the RRM, hereafter referred to as the Mid domain) induced repression (Fig. 1*C*, Mid). On the other hand, no significant repression was observed with TNRC6A fragments lacking the Mid domain despite detectable expression of effector proteins (Fig. 1*F*). The repression was mediated via specific binding of N-peptide fusions to BoxB sequences (Fig. S1). qRT-PCR showed that mRNA stability was not changed by tethered TNRC6A proteins during the assay (Fig. 1*D*). RNaseH-mediated poly(A) tail analysis revealed that the full-length TNRC6A, the silencing domain fragment and the Mid domain fragment induced deadenylation (Fig. 1*E*). These results reveal that the Mid domain of zebrafish TNRC6A is essential and sufficient to induce translational inhibition and deadenylation.

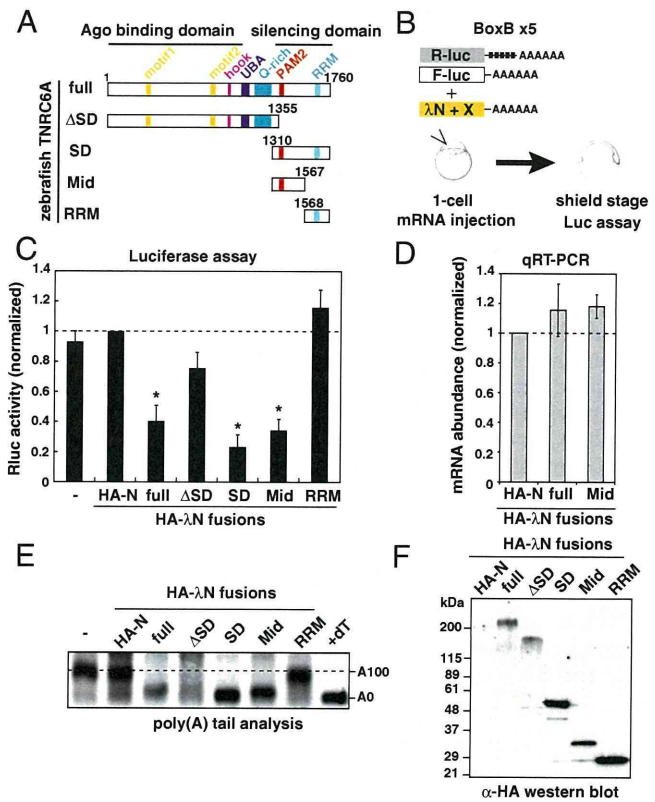

Fig. 1. The Mid domain of TNRC6A is sufficient to induce translational repression and deadenylation. (*A*) Schematic structures of zebrafish TNRC6A and its deletion mutants. (*B*) Schematic representation of the λN tethering assay in zebrafish embryos. (*C*) Results of the tethering assay with TNRC6A fragments. The bar graph shows Rluc activity that was normalized to Fluc activity. The normalized Rluc activity with the HA-λN empty construct (HA-N) was set to one. The data show averages of three independent experiments. Error bars show SD. Asterisks indicate $p < 0.01$ compared to experiments with HA-N. (*D*) The qRT-PCR analysis of reporter mRNA stability. The normalized Rluc mRNA values [normalized to those of the HA-λN empty construct (HA-N)] were set to one. The data show averages of three independent experiments. Error bars show SD. (*E*) The poly(A) tail analysis of the Rluc-BoxB-pA reporter mRNA by RNaseH digestion and Northern blot. The lane +dT shows completely deadenylated fragments, which correspond to A0. (*F*) Western blotting detecting HA-tagged effecter proteins.

A Previously Undescribed P-GL Motif in TNRC6A Contributes to Translational Inhibition in Concert with the PAM2 Motif. The PAM2 motif was conserved in the Mid domain of zebrafish TNRC6A, with critical residues for the interaction with PABP remaining invariant (Fig. 2*A*) (18–20). To determine whether the silencing activities of the Mid domain required PAM2–PABP interaction, we introduced a mutation into the PAM2 motif of the TNRC6A Mid domain (Fig. 2*A*, E1421 and F1422 to A; PAM2 mutation). The PAM2 mutation completely abolished the interaction with PABP, which was assessed using the GST-pulldown assay with zebrafish embryo lysates (Fig. 2*B*). In the tethering assay, the PAM2 mutation slightly reduced repression activity (Fig. 2 *C* and *D*, $p < 0.05$). Deadenylation of the Rluc-BoxB-poly(A) mRNA was still induced by the PAM2 mutant in this context (Fig. 2*E*). These results indicate that TNRC6 silencing activity is mediated by the PAM2 motif as suggested in the previous studies (18, 20), yet the contribution might not be predominant in zebrafish embryos.

To characterize repression activities that remained in the PAM2 mutant, we focused on the residues PPPGLT, which are located at the C terminus of the Mid domain and are highly conserved in the TNRC6 family proteins (hereafter referred to as the P-GL motif, Fig. 2*A*). A mutation introduced into this motif (G1544 and L1545 to A; P-GL mutation) did not affect PABP interaction (Fig. 2*B*). On the contrary, the P-GL mutation partially reduced the repression activity of the Mid domain ($p < 0.01$) with no obvious effect on deadenylation (Fig. 2 *C* and *E*, P-GL mut). Repression activity of the Mid domain was further impaired when the PAM2 and P-GL motifs were simultaneously mutated (Fig. 2*C*, PAM2/P-GL mut). Concomitantly, the deade-

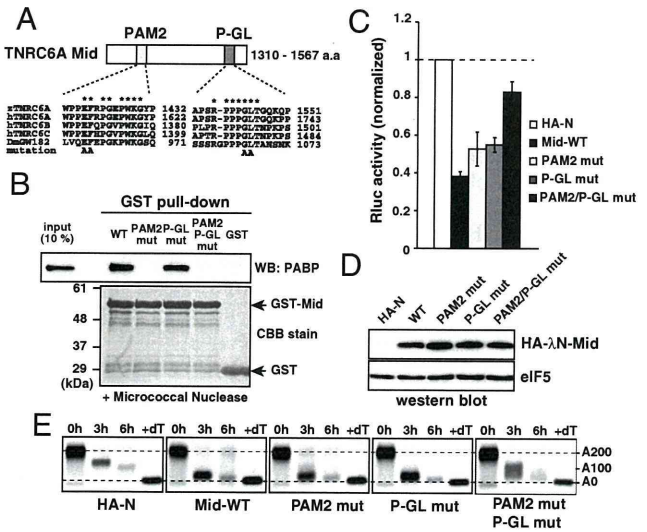

Fig. 2. The Mid domain of TNRC6A represses translation via two motifs. (*A*) Schematic representation of the Mid domain of zebrafish TNRC6A. The two conserved motifs (PAM2 and P-GL) are shown. Sequence alignments of each motif comparing zebrafish TNRC6A, human TNRC6 proteins, and fly GW182 are shown. Conserved residues are marked with asterisks. Alanine substitutions introduced in the current study are shown on the bottom. (*B*) GST-pulldown assay detecting interaction between the GST-Mid domain and zebrafish PABP. A total of 10% of embryonic lysate was loaded as an input. PABP was detected using Western blotting (*Upper*). GST fusion proteins were visualized using CBB stain (*Lower*). (*C*) The results of the tethering assay with TNRC6A Mid domain mutants. The data were collected and are shown as described in Fig. 1*C*. (*D*) Western blot detecting HA-λN-tagged Mid domain proteins. The membrane was probed with anti-eIF5 antibody as a control. (*E*) The poly(A) tail analysis of the injected Rluc-BoxB-pA reporter mRNA using RNaseH digestion and northern blot at 0, 3 and 6 hours. The lane +dT shows a completely deadenylated fragment (A0).

nylation activity was reduced in the double mutant (Fig. 2*E*). These results suggested that a previously undescribed P-GL motif in the Mid domain contributes to the translational inhibition in concert with the PAM2 motif.

To test the contributions of PAM2 and P-GL motifs in the context of full-length TNRC6A function, we performed two experiments. First, we introduced the mutations into the full-length TNRC6A and tested their effects in the tethering assay (Fig. S2 *A–C*). The simultaneous loss of both PAM2 and P-GL motifs, but not the loss of one of the two motifs, strongly impaired the repression activity of TNRC6A at translation level. Second, to test the activity of TNRC6A variants in the context of miRNA-mediated repression, we asked if exogenous TNRC6A variants enhance miR-430-mediated repression of the GFP sensor transgene (Fig. S2*D*; see Fig. 5 for detailed information of the GFP-miR-430 sensor). Overexpression of wild-type, PAM2 mutant, and P-GL mutant versions of TNRC6A promoted miR-430-mediated repression of the GFP-miR-430 sensor. In contrast, the double mutant failed to promote repression by miR-430 (Fig. S2 *E* and *F*). These two experiments indicated that our motif analysis with the Mid domain fragment well captured the actions of the full-length TNRC6A.

TNRC6A Mediates Translational Inhibition Independent of Deadenylation. Given the predominant contribution of the PAM2 and the P-GL motifs to translational inhibition with the moderate effect on deadenylation, we next asked if the translational inhibition induced by these two motifs was independent of deadenylation. To this end, we performed two experiments. First, we analyzed the physical interactions between the Mid domain and deadenylase components that have been implicated in miRNA-mediated deadenylation (18, 21, 23, 24). Consistent with its deadenylation activity in the tethering assay, the GST-Mid domain interacted with in vitro translated Myc-tagged PAN3 and CCR4/CAF1 but not with eIF4E (Fig. 3*A* and Fig. S3 *A* and *B*). Notably, the PAM2/P-GL double mutant still interacted with these factors with reduced affinity to PAN3. Second, we asked whether the Mid domain induced translational repression in the absence of deadenylation. To this end, we generated a synthetic poly(A) tail that contained a 98 nt poly(A) sequence followed by a 10 nt poly(C) sequence (A98C10, Fig. 3*B*). The A98C10 tail was not deadenylated by the Mid domain during the assay (Fig. 3*C*). On the other hand, the A98C10 tail enhanced Rluc expression similar to the normal poly(A) tail (Fig. S4*A*). Tethering experiments revealed that the Mid domain strongly silenced tethered mRNA with the A98C10 tail. Furthermore, the coordinated contribution of the PAM2 and P-GL motifs was observed with the A98C10 tail (Fig. 3*D*). These experiments showed that the Mid domain of TNRC6A inhibited translation via the PAM2 and P-GL motifs in a deadenylation-independent manner.

The PAM2 and P-GL Motifs Contribute to Translational Silencing Through Distinct Mechanisms. Next, we determined whether the PAM2 and P-GL motifs required PABP for their function in translation repression. To this end, we utilized Paip2 (PABP-interacting protein 2). Paip2 binds to PABP via its PAM1 and PAM2 motifs, and sequesters PABP by displacing it from the poly(A) tail and eIF4G (25). Hence, we predicted that the repression by the Mid domain would be diminished by Paip2 if PABP is the only molecular target for the Mid domain. First we confirmed that the A98C10 tail failed to stimulate translation in the presence of excess Paip2 (Fig. S4*B*). In the presence of excess Paip2, the Mid domain repressed translation of Rluc-BoxB-A98C10 mRNA (Fig. 3*E*). This result suggests that the Mid domain inhibits translation via a PABP-independent mechanism. Consistent with this idea, the Mid domain with the PAM2 mutation inhibited translation of Rluc-BoxB-A98C10 mRNA similar to the wild-type Mid domain ($p > 0.38$). In contrast, the P-GL mutation diminished

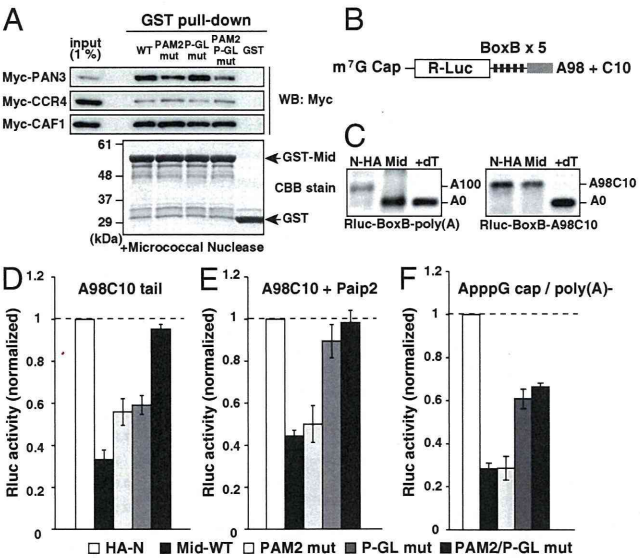

Fig. 3. The Mid domain of TNRC6A represses translation via deadenylation-independent mechanisms. (*A*) The GST-pulldown assay detecting interactions between the GST-Mid domain and deadenylase components translated in rabbit reticulocyte lysate. Total of 1% of in vitro translation reaction was loaded as an input. Myc-tagged proteins were detected using Western blotting (*Upper*). GST fusion proteins were visualized using CBB stain (*Lower*). (*B*) Rluc reporter mRNA containing 5 copies of BoxB sites followed by the A98C10 tail. (*C*) The poly(A) tail analysis of the Rluc-BoxB reporter mRNAs at six hours, in the presence of control HA-λN peptide (HA-N) or the HA-λN tagged Mid domain (Mid). *Left*: The reporter mRNA with a normal poly(A) tail [Rluc-BoxB-poly(A)]. *Right*: The reporter mRNA with an A98C10 tail (Rluc-BoxB-A98C10). The lane +dT shows a completely deadenylated fragment (A0). (*D*) Tethering assay of the TNRC6A Mid domain with reporter mRNA containing the A98C10 tail in the presence of Myc-GFP. (*E*) Tethering assay of the TNRC6A Mid domain with reporter mRNA containing the A98C10 tail in the presence of Myc-Paip2. (*F*) Tethering assay of the TNRC6A Mid domain constructs with a reporter mRNA containing the 5′ ApppG cap without a poly(A) tail. Graphs in *D*, *E*, and *F* show the averages of three independent experiments. Error bars show SD.

most of the repressive effect caused by the Mid domain in the presence of Paip2. Hence, the PAM2 motif required PABP for translational inhibition, while the P-GL motif did not. As an alternative approach, we determined whether the m^7G cap and the poly(A) tail, which are two important constituents for translation initiation, are required for translational inhibition by the Mid domain. Although the translation efficiency was significantly reduced in the absence of the m^7G cap and the poly(A) tail (Fig. S4*A*), the tethering assay revealed that the Mid domain repressed bound mRNA even in the absence of the m^7G cap and poly(A) tail (Fig. 3*F*). Analysis with Mid domain mutants showed that the P-GL motif, but not the PAM2 motif, contributed to repression of this reporter mRNA. The contribution of the P-GL motif was not attributed to the change in the RNA stability (Fig. S4*C*), indicating that the P-GL motif inhibited translation. These results strongly suggested that the Mid domain of TNRC6A inhibits translation through two distinct mechanisms.

Direct Translational Inhibition Is a Major Output of miRNA-Mediated Repression During Zebrafish Embryogenesis. To validate our findings obtained in the tethering assay, we designed a miRNA reporter system in zebrafish embryos using a firefly luciferase (Fluc) mRNA containing the 3′UTR of an endogenous miR-1 target gene, pdlim1 (26) (Fig. 4*A*). The Fluc-pdlim1 mRNA and a non-targeted mRNA encoding Renila luciferase (Rluc) were microinjected into fertilized eggs together with the miR-1 duplex or control miR-124 duplex. Six or 10 h after the injection, a luciferase assay and quantitative RT-PCR (qRT-PCR) were performed

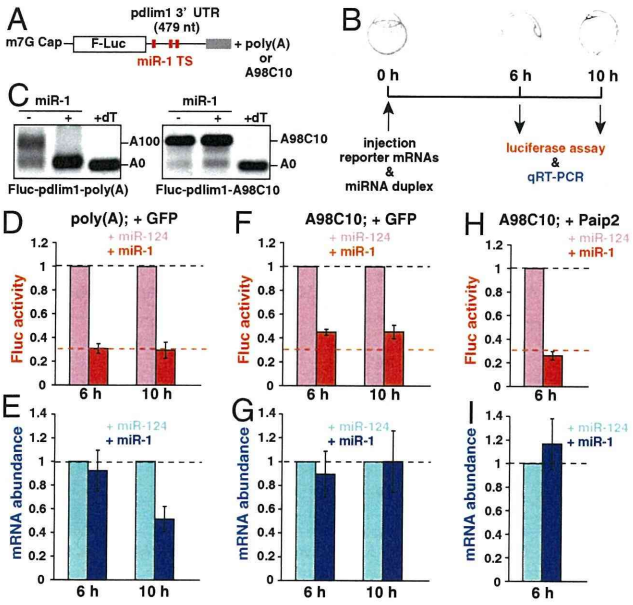

Fig. 4. miR-1 represses target mRNA in a deadenylation- and PABP-independent manner in zebrafish embryos. (*A*) Fluc reporter mRNA containing zebrafish pdlim1 3′UTR. Red boxes indicate the target site for miR-1. (*B*) Scheme of the miR-1 repression assay in zebrafish embryos. (*C*) The poly(A) tail analysis of the Fluc-pdlim1 3′UTR reporter mRNAs at six hours in the absence (–) or presence (+) of the miR-1 duplex. The left panel shows the reporter mRNA with a normal poly(A) tail [Fluc-pdlim1-poly(A)]. The right panel shows the reporter mRNA with the A98C10 tail (Fluc-pdlim1-A98C10). (*D* and *E*) The results of the miR-1 repression assay with reporter mRNA containing a normal poly(A) tail in the presence of control Myc-GFP. (*F* and *G*) Results of the miR-1 repression assay with reporter mRNA containing the A98C10 tail in the presence of control Myc-GFP. (*H* and *I*) Results of the miR-1 repression assay with reporter mRNA containing the A98C10 tail in the presence of Myc-Paip2. *D*, *F*, and *H* show normalized Fluc activity. *E*, *G*, and *I* show normalized Fluc mRNA levels, which were measured using qRT-PCR. The values of the experiments using miR-124 were set to one at each time point. The data shows averages of three independent experiments. Error bars show SD.

to measure protein expression and mRNA stability (Fig. 4*B*). As observed in the tethering assay, the A98C10 tail resisted deadenylation by miR-1 in this system (Fig. 4*C*).

The analysis using Fluc-pdlim1 mRNA with the normal poly (A) tail revealed strong repression of Fluc activity by miR-1 at 6 h (to approximately 30% compared to the miR-124 duplex), with no obvious change in mRNA abundance (Fig. 4 *D* and *E*, 6 h). Substantial mRNA degradation by miR-1 was detected at 10 h. However, miR-1-mediated mRNA reduction (approximately 50% compared to miR-124) does not fully account for the overall repressive effect of miR-1, which was measured by the luciferase activity (approximately 30%) (Fig. 4 *D* and *E*, 10 h). These results suggest a major contribution of translational inhibition in the miRNA pathway during zebrafish embryogenesis. To validate the contribution of deadenylation to miRNA-mediated repression, we performed the miR-1 repression assay with the deadenylation-resistant A98C10 tail. This analysis revealed two important findings. First, miR-1 inhibited translation of Fluc-pdlim1 mRNA with the A98C10 tail with a lower efficiency compared to the Fluc-pdlim1 mRNA with the normal poly(A) tail (approximately 45% with the A98C10 tail, versus approximately 30% with the normal poly(A) tail at 6 h; Fig. 4*F*). Second, the A98C10 tail inhibited miR-1-mediated Fluc mRNA degradation during the assay (Fig. 4*G*). These analyses confirmed a major contribution of deadenylation-independent translational inhibition during miRNA-mediated repression. Next, we analyzed the involvement of PABP-related mechanism in miRNA-mediated translational inhibition. Inhibition of PABP by Paip2 did not abrogate miR-1-mediated repression. Rather, it promoted miR-1-mediated translational inhibition of the Fluc-pdlim1-A98C10 mRNA to approximately 30% (Fig. 4 *H* and *I*). Hence, miR-1 can induce translation repression in parallel to the PABP inhibiton by Paip2. These results reveal distinct contributions of deadenylation, PABP inhibition, and PABP-independent translational inhibition to miRNA-mediated repression in vivo.

A PABP-Independent Mechanism of miRNA-Mediated Repression Operates During Zebrafish Embryogenesis. To further confirm whether miRNA inhibited its target mRNA via PABP-independent repression pathways in vivo, we depleted PABP from zebrafish embryos and analyzed the effects on miRNA-mediated repression. Among zebrafish orthologues of vertebrate PABP genes, the expression of two PABPC1 paralogues (pabpc1a and pabpc1b) and PABPC4 was detected during zebrafish embryogenesis (Fig. 5*A* and Fig. S5*A*). Although pabpc1a mRNA was ubiquitously expressed during development, the expression of pabpc1b and pabpc4 mRNAs was restricted to specific tissues at 24 h post fertilization (hpf). Injection with the translation-blocking morpholino oligo (MO) for pabpc1a mRNA at the one-cell stage reduced total PABP levels to <1% compared to the injection of embryos with control MO (Fig. 5*B* and Fig. S5*B*; note that the antibody we used detected all three PABP proteins described above). Concomitantly, PABP-depleted embryos showed reduced formation of polysomes (Fig. 5*C*) and strong morphological defects (Fig. 5*D*, upper panels) at 24 hpf. Therefore, cellular PABP was reduced to nonfunctional levels in pabpc1a MO-injected embryos.

To monitor endogenous miRNA-mediated repression, we generated a transgenic zebrafish that ubiquitously expressed GFP mRNA containing three copies of the miR-430 target site (TS) [Tg(ßactin-GFP-3xTS-miR-430)]. Expression of GFP protein from this reporter gene was strongly repressed throughout the embryo by the ubiquitous miRNA miR-430 in a target-site dependent manner (Fig. 5*D*, middle panels) (9, 27). Notably, miR-430 repressed the GFP reporter in PABP-depleted embryos. In situ hybridization revealed concomitant degradation of the reporter mRNA (Fig. 5*D*, lower panels), indicating that the repressive effect we observed in the transgenic embryos might be a combined output of initial translational repression and subsequent mRNA degradation. Similar findings were observed with another GFP transgenic line that visualized repression by muscle specific miRNA miR-1/206 (26) (Fig. S6). The PABP-depletion did not cause shortening of the basal poly(A) tail length as a secondary effect (Fig. 5*F*). These results with the transgenic lines, together with the results with injected reporter mRNAs in Fig. 4, show that miRNA silences its target mRNA via PABP-independent mechanism(s) during zebrafish embryogenesis.

Discussion

Due to its intricate outputs, it has been difficult to delineate the direct and primary consequence of miRNA-mediated repression (3, 11). In this study, we addressed a causal relationship between miRNA-mediated translational repression and deadenylation using three different approaches. First, we revealed that the PAM2 and P-GL motifs in the Mid domain of zebrafish TNRC6A induced translational inhibition in a deadenylation-independent manner (Figs. 2*C* and 3*D*). Second, we found that the Mid domain carrying the PAM2 and P-GL mutations showed reduced affinity to PAN3 but still interacted with CCR4/CAF1 deadenylases (Fig. 3*A* and Fig. S3 *A* and *B*). Third, miR-1 induced translational repression of its target reporter mRNA even in the absence of deadenylation (Fig. 4*F*). These observations collectively indicate that miRNA-mediated translational inhibition and deadenylation are independent outputs mediated through distinct molecular actions of TNRC6.

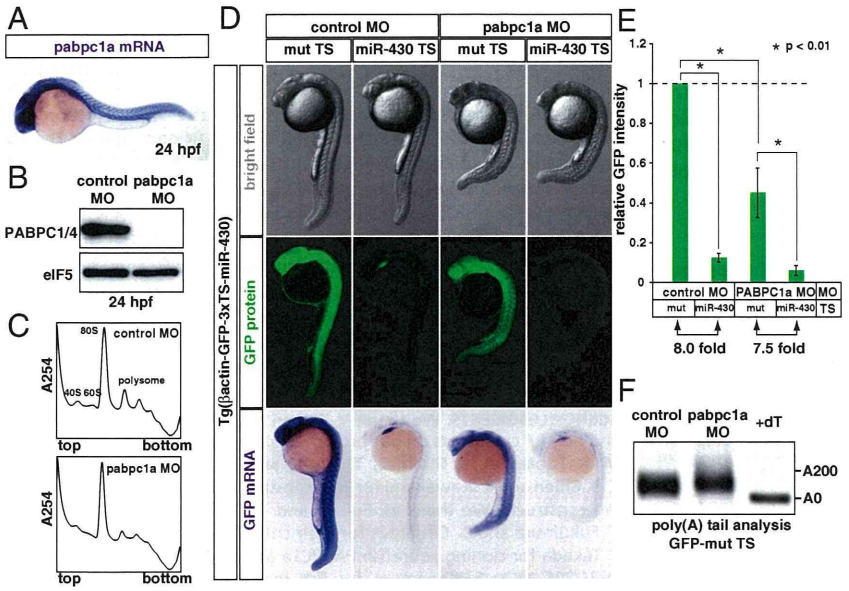

Fig. 5. miR-430 represses its target mRNA in the absence of PABP during zebrafish embryogenesis. (*A*) In situ hybridization detecting pabpc1a mRNA in a 24 hpf zebrafish embryo (purple). (*B*) Western blot detecting PABP protein in 24 hpf embryos injected with control MO or pabpc1a MO. The membrane was probed with anti-eIF5 antibody as a control. (*C*) The polysome profiles of control MO-injected (*Upper*) and pabpc1 MO-injected (*Lower*) zebrafish embryos at 24 hpf. (*D*) Analysis of miRNA-mediated target mRNA repression in the presence or absence of PABP. Bright field view (*Upper* panels), GFP fluorescence (*Middle* panels; green) and GFP mRNA (*Bottom* panels; purple) of 24 hpf zebrafish embryos expressing the GFP transgene with three copies of the imperfect target site for the ubiquitously expressed miRNA, miR-430 (miR-430 TS) or with mutated target sites (mut TS). Control MO (left columns) or pabpc1a MO (right columns) was injected as indicated. (*E*) Quantification of GFP expression levels in Fig. 5*D*. GFP intensity of the embryos with the mut TS and the control MO was set to one. Error bars show SD. Asterisks indicate $p < 0.01$ compared to the experiment with the mut TS and control MO. (*F*) The poly(A) tail analysis of the GFP mut TS mRNA with the control MO or pabpc1a MO. The lane +dT shows a completely deadenylated fragment (A0).

The use of the deadenylation-resistant A98C10 tail allowed us to determine the relative contributions of direct translational inhibition and deadenylation in the miRNA pathway. Although we observed the contribution of deadenylation to miR-1-mediated translational inhibition, we also observed substantial translational inhibition in the absence of deadenylation with miR-1 and the tethered Mid domain (Figs. 3*D* and 4*F*). These observations establish that translational inhibition by miRNA is not a mere consequence of deadenylation. Consistent with these findings, mRNAs that were translated in a poly(A) tail-independent manner were repressed by miRNA (10, 21). Hence, we propose that deadenylation plays an auxiliary role in the miRNA-mediated repression by consolidating translational inhibition, possibly through displacement of PABP from mRNA. We also observed that miRNA required deadenylation for target mRNA degradation that occurred at a later time point (Fig. 4*E*, 10 h). Therefore, we do not exclude the possibility that deadenylation and subsequent mRNA degradation play more active roles in miRNA-mediated silencing after extended periods, which has been suggested by previous genome-wide analyses (6–8). Nevertheless, a rapid and strong translational inhibition in our zebrafish system supported a model in which direct translational inhibition is central to miRNA-mediated gene silencing at early time points.

The mechanisms that mediate direct translational repression by miRNA have not been well characterized. Some of our data are consistent with a model in which miRNA/TNRC6 induces silencing by interacting with PABP via its PAM2 motif (11). In our tethering assay, the PAM2 motif in the Mid domain of zebrafish TNRC6A contributed to translational inhibition when PABP was involved in translation (Fig. 2*C*). This contribution was deadenylation-independent (Fig. 3*D*), indicating that the PAM2 motif contributed to translational inhibition by counteracting the function of PABP in translation. These observations are also consistent with previous studies arguing that miRNA targets the m^7G cap-dependent translation initiation process (28–31). In addition, our study indicated that the PAM2–PABP interaction was not the only mechanism used by miRISC to inhibit translation. First, the mutation into the PAM2 motif only weakly reduced the repression activity of the Mid domain (Figs. 2 and 3) and the full-length TNRC6A (Fig. S2). Second, miR-1 and the Mid domain induced translational inhibition even in a PABP-independent manner (Figs. 3*E* and 4*F*). Third, depletion of PABP from zebrafish embryos allowed endogenous miRNAs to silence their target mRNAs (Fig. 5 and Fig. S6). Hence, zebrafish miRISC is equipped with a mechanism that does not require PABP for target mRNA silencing. In contrast, previous studies in mammalian cultured cells have shown correlations between cellular PABP activity and miRNA-mediated repression (20, 32). It is therefore possible that the contribution of the PAM2–PABP interaction to miRNA-mediated repression is conditional on the general translation status in the cell.

We identified a previously undescribed conserved motif, the P-GL motif, which was within the Mid domain of TNRC6A, as a PABP-independent translation repression mechanism. The action of the P-GL motif was clearly distinct from that of the PAM2 motif in three aspects. First, the P-GL motif was not involved in PABP binding (Fig. 2*B*). Second, the P-GL motif contributed to translational repression irrespective of the presence of poly(A) tail or the PABP activity (Figs. 3*E* and *F*). Third, the P-GL motif contributed to the repression of mRNA with the unnatural 5′ ApppG cap structure (Fig. 3*F*). Hence, the P-GL motif repressed mRNA translation independent of essential constituents of the canonical translation initiation pathway. Because the use of the ApppG cap structure significantly reduced the basal translation activity (Fig. S4*A*), the exact contribution and the molecular basis of the observed repression activity need to be interpreted in the context of the m^7G capped and polyadenylated mRNA. Nevertheless, it is worth noticing that the cap-independent repression activity observed with the P-GL motif is consistent with post-initiation repression models of miRNA (33–36). Based on these observations, we propose a "double lock model" of miRNA-mediated translational repression, in which miRNA inhibits two distinct translation steps through TNRC6 (Fig. S7).

While this manuscript was under revision, three papers reported additional functional motifs in fly GW182 and mammalian TNRC6 proteins that mediate binding to the CCR4/NOT1 and PAN2/PAN3 deadenylase complexes (37–39). Interestingly, those complexes induced repression not only via deadenylation but also via deadenylation-independent mechanism(s) (37, 39). Moreover, Fukaya and Tomari recently reported that, consistent with our findings in zebrafish, miRNA induces translation repression independent of deadenylation and PABP in the fly in vitro system (40). Although the relative contributions of these pathways need to be clarified, our current study and these recent reports collec-

tively indicate that miRNA system utilizes multiple redundant mechanisms to silence target mRNAs. The characterization of multiple translational inhibition activities of TNRC6 proteins in a wide variety of experimental systems may reconcile contradicting observations on miRNA-mediated translational inhibition (3, 11). It is tempting to speculate that, by having multiple repression mechanisms, miRNA performs robust control of target gene expression under diverse cellular contexts.

Materials and Methods

Tethering Assay in Zebrafish Embryos. The mRNAs were transcribed using an mMessage mMachine SP6 kit (Ambion). ApppG capped mRNA was synthesized in the presence of an ApppG cap analogue (New England Biolabs) instead of an m^7GpppG cap analogue. To add a normal poly(A) tail, the mRNA was polyadenylated in vitro using a poly(A) tailing kit (Ambion). For poly(A)- mRNA, we injected a MO that binds to the end of the mRNA to inhibit polyadenylation (TB-MO). For mRNA injections, Rluc mRNA and Fluc mRNA were diluted to a final concentration of 50 ng/μL each. Effector mRNAs were diluted to obtain solutions with equimolar concentrations of effector mRNA. HA-λN-Mid mRNA was diluted to a final concentration of 100 ng/μL. The mRNA encoding myc-tagged GFP or zebrafish Paip2 was added to a final concentration of 200 ng/μL. Approximately 1,000 pl of solution containing reporter mRNAs and effecter mRNAs was injected into one-cell stage zebrafish embryos. A total of 5–10 embryos were collected at the shield stage (6 hpf) and lysed in Passive lysis buffer (Promega). The luciferase activities were measured using the Dual-Luciferase Reporter assay system and GloMax 20/20 n luminometer (Promega). Rluc activity intensity (IRluc) was normalized to the intensity of Fluc activity (IFluc). The normalized Rluc activity for each experiment with HA-N effector encoding XX was calculated as follows. Fold change = (IFluc + HA-N-XX/IRluc + HA-N-XX)/(IFluc-control/IRluc-control). The values obtained using HA-N empty mRNA were used for controls. Each sample was measured as three replicates. The p value was calculated using Student's t test.

qRT-PCR. A total of five embryos were retained after each injection experiment, and total RNA was extracted by ISOGEN (Nippon gene). The cDNA was synthesized using the PrimeScript RT reagent kit (TAKARA). A random hexamer was used for cDNA synthesis to avoid detecting differences in the poly(A) tail length. To assess Fluc mRNA and Rluc mRNA levels, qRT-PCR was performed with SYBR Premix EX Taq II and the Thermal Cycler Dice Real Time System (TAKARA) following a standard protocol. Specific amplification of the PCR products was confirmed by analyzing the dissociation curve, running the products on an agarose gel, and sequencing. Each sample was measured as duplicates, and each experiment was repeated three times.

Additional materials and methods are described in *SI Text*.

ACKNOWLEDGMENTS. We thank Y. Tomari and M. W. Hentze for discussions and helpful comments on our project. We are also grateful to N. Sonenberg, M. R. Fabian, A. J. Giraldez, T. Inada, and M. Wakiyama for discussions; C. B. Chien and K. Kawakami for Tol2 constructs; and A. Kulozik for λN tethering constructs. We thank H. Fukaki and T. Goh for their help in qRT-PCR; K. Fukumura and D. Cifuentes for their critical comments on the manuscript; Y. Takeda for cloning zebrafish PABPC1a and Paip2; R. Kusakabe for sharing miR1/206 MOs; S. Kanamura for fish maintenance; and members of our laboratory for their support. This work was supported by Grants-in-Aid for Scientific Research from Japan Ministry of Education, Culture, Sports, Science and Technology to Y.M (22115510) and K.I (20112003), the Uehara Memorial Foundation and the Senri Life Science Foundation to Y.M, and the Asahi Glass Foundation to K.I. A.F. is a research fellow of the Japan Society for the Promotion of Science.

1. Bushati N, Cohen SM (2007) microRNA functions. *Annu Rev Cell Dev Biol* 23:175–205.
2. Bartel DP (2009) MicroRNAs: Target recognition and regulatory functions. *Cell* 136:215–233.
3. Fabian MR, Sonenberg N, Filipowicz W (2010) Regulation of mRNA translation and stability by microRNAs. *Annu Rev Biochem* 79:351–379.
4. Lim LP, et al. (2005) Microarray analysis shows that some microRNAs downregulate large numbers of target mRNAs. *Nature* 433:769–773.
5. Giraldez AJ, et al. (2006) Zebrafish MiR-430 promotes deadenylation and clearance of maternal mRNAs. *Science* 312:75–79.
6. Guo H, Ingolia NT, Weissman JS, Bartel DP (2010) Mammalian microRNAs predominantly act to decrease target mRNA levels. *Nature* 466:835–840.
7. Hendrickson DG, et al. (2009) Concordant regulation of translation and mRNA abundance for hundreds of targets of a human microRNA. *PLoS Biol* 7:e1000238.
8. Selbach M, et al. (2008) Widespread changes in protein synthesis induced by microRNAs. *Nature* 455:58–63.
9. Mishima Y, et al. (2006) Differential regulation of germline mRNAs in soma and germ cells by zebrafish miR-430. *Curr Biol* 16:2135–2142.
10. Wu L, Fan J, Belasco JG (2006) MicroRNAs direct rapid deadenylation of mRNA. *Proc Natl Acad Sci USA* 103:4034–4039.
11. Huntzinger E, Izaurralde E (2011) Gene silencing by microRNAs: contributions of translational repression and mRNA decay. *Nat Rev Genet* 12:99–110.
12. Hutvagner G, Simard MJ (2008) Argonaute proteins: Key players in RNA silencing. *Nat Rev Mol Cell Biol* 9:22–32.
13. Eulalio A, Tritschler F, Izaurralde E (2009) The GW182 protein family in animal cells: New insights into domains required for miRNA-mediated gene silencing. *RNA* 15:1433–1142.
14. Behm-Ansmant I, et al. (2006) mRNA degradation by miRNAs and GW182 requires both CCR4:NOT deadenylase and DCP1:DCP2 decapping complexes. *Genes Dev* 20:1885–1898.
15. Till S, et al. (2007) A conserved motif in Argonaute-interacting proteins mediates functional interactions through the Argonaute PIWI domain. *Nat Struct Mol Biol* 14:897–903.
16. Eulalio A, Helms S, Fritzsch C, Fauser M, Izaurralde E (2009) A C-terminal silencing domain in GW182 is essential for miRNA function. *RNA* 15:1067–1077.
17. Lazzaretti D, Tournier I, Izaurralde E (2009) The C-terminal domains of human TNRC6A, TNRC6B, and TNRC6C silence bound transcripts independently of Argonaute proteins. *RNA* 15:1059–1066.
18. Fabian MR, et al. (2009) Mammalian miRNA RISC recruits CAF1 and PABP to affect PABP-dependent deadenylation. *Mol Cell* 35:868–880.
19. Jinek M, Fabian MR, Coyle SM, Sonenberg N, Doudna JA (2010) Structural insights into the human GW182-PABC interaction in microRNA-mediated deadenylation. *Nat Struct Mol Biol* 17:238–240.
20. Huntzinger E, Braun JE, Heimstadt S, Zekri L, Izaurralde E (2010) Two PABPC1-binding sites in GW182 proteins promote miRNA-mediated gene silencing. *EMBO J* 29:4146–4160.
21. Eulalio A, et al. (2009) Deadenylation is a widespread effect of miRNA regulation. *RNA* 15:21–32.
22. Zipprich JT, Bhattacharyya S, Mathys H, Filipowicz W (2009) Importance of the C-terminal domain of the human GW182 protein TNRC6C for translational repression. *RNA* 15:781–793.
23. Piao X, Zhang X, Wu L, Belasco JG (2010) CCR4-NOT deadenylates mRNA associated with RNA-induced silencing complexes in human cells. *Mol Cell Biol* 30:1486–1494.
24. Chen CY, Zheng D, Xia Z, Shyu AB (2009) Ago-TNRC6 triggers microRNA-mediated decay by promoting two deadenylation steps. *Nat Struct Mol Biol* 16:1160–1166.
25. Sonenberg N, Dever TE (2003) Eukaryotic translation initiation factors and regulators. *Curr Opin Struct Biol* 13:56–63.
26. Mishima Y, et al. (2009) Zebrafish miR-1 and miR-133 shape muscle gene expression and regulate sarcomeric actin organization. *Genes Dev* 23:619–632.
27. Giraldez AJ, et al. (2005) MicroRNAs regulate brain morphogenesis in zebrafish. *Science* 308:833–838.
28. Pillai RS, et al. (2005) Inhibition of translational initiation by Let-7 MicroRNA in human cells. *Science* 309:1573–1576.
29. Humphreys DT, Westman BJ, Martin DI, Preiss T (2005) MicroRNAs control translation initiation by inhibiting eukaryotic initiation factor 4E/cap and poly(A) tail function. *Proc Natl Acad Sci USA* 102:16961–16966.
30. Mathonnet G, et al. (2007) MicroRNA inhibition of translation initiation in vitro by targeting the cap-binding complex eIF4F. *Science* 317:1764–1767.
31. Thermann R, Hentze MW (2007) Drosophila miR2 induces pseudo-polysomes and inhibits translation initiation. *Nature* 447:875–878.
32. Walters RW, Bradrick SS, Gromeier M (2010) Poly(A)-binding protein modulates mRNA susceptibility to cap-dependent miRNA-mediated repression. *RNA* 16:239–250.
33. Olsen PH, Ambros V (1999) The lin-4 regulatory RNA controls developmental timing in Caenorhabditis elegans by blocking LIN-14 protein synthesis after the initiation of translation. *Dev Biol* 216:671–680.
34. Wang B, Yanez A, Novina CD (2008) MicroRNA-repressed mRNAs contain 40S but not 60S components. *Proc Natl Acad Sci USA* 105:5343–5348.
35. Petersen CP, Bordeleau ME, Pelletier J, Sharp PA (2006) Short RNAs repress translation after initiation in mammalian cells. *Mol Cell* 21:533–542.
36. Nottrott S, Simard MJ, Richter JD (2006) Human let-7a miRNA blocks protein production on actively translating polyribosomes. *Nat Struct Mol Biol* 13:1108–1114.
37. Braun JE, Huntzinger E, Fauser M, Izaurralde E (2011) GW182 proteins directly recruit cytoplasmic deadenylase complexes to miRNA targets. *Mol Cell* 44:120–133.
38. Fabian MR, et al. (2011) miRNA-mediated deadenylation is orchestrated by GW182 through two conserved motifs that interact with CCR4-NOT. *Nat Struct Mol Biol* 18:1211–1217.
39. Chekulaeva M, et al. (2011) miRNA repression involves GW182-mediated recruitment of CCR4-NOT through conserved W-containing motifs. *Nat Struct Mol Biol* 18:1218–1226.
40. Fukaya T, Tomari Y (2011) PABP is not essential for microRNA-mediated translational repression and deadenylation in vitro. *EMBO J*, 10.1038/emboj.2011.426.

Published online 17 January 2012

Nucleic Acids Research, 2012, Vol. 40, No. 8 ***e58***
doi:10.1093/nar/gkr1317

A potent 2′-*O*-methylated RNA-based microRNA inhibitor with unique secondary structures

Takeshi Haraguchi[1], Haruo Nakano[2], Takanobu Tagawa[1], Tokimitsu Ohki[3], Yoshihito Ueno[4], Tetsuo Yoshida[2] and Hideo Iba[1,*]

[1]Division of Host-Parasite Interaction, Department of Microbiology and Immunology, Institute of Medical Science, University of Tokyo, 4-6-1 Shirokanedai, Minato-ku, Tokyo 108-8639, [2]Inovative Drug Research Laboratories, Kyowa Hakko Kirin Co., Ltd., 3-6-6, Asahi-machi, Machida-shi, Tokyo 194-8533 and [3]Department of Biomolecular Science, Faculty of Engineering and [4]Department of Applied Life Science, Faculty of Applied Biological Sciences, Gifu University, 1-1 Yanagido, Gifu 501-1193, Japan

Received May 19, 2011; Revised December 7, 2011; Accepted December 23, 2011

ABSTRACT

MicroRNAs (miRNAs) are involved in various biological processes and human diseases. The development of strong low-molecular weight inhibitors of specific miRNAs is thus expected to be useful in providing tools for basic research or in generating promising new therapeutic drugs. We have previously described the development of 'Tough Decoy (TuD) RNA' molecules, which achieve the long-term suppression of specific miRNA activity in mammalian cells when expressed from a lentivirus vector. In our current study, we describe new synthetic miRNA inhibitors, designated as S-TuD (Synthetic TuD), which are composed of two fully 2′-*O*-methylated RNA strands. Each of these strands includes a miRNA-binding site. Following the hybridization of paired strands, the resultant S-TuD forms a secondary structure with two stems, which resembles the corresponding TuD RNA molecule. By analyzing the effects of S-TuD against miR-21, miR-200c, miR-16 and miR-106b, we have elucidated the critical design features of S-TuD molecules that will provide optimum inhibitory effects following transfection into human cell lines. We further show that the inhibitory effects of a single transfection of S-TuD-miR200c are quite long-lasting (>7 days) and induce partial EMT, the full establishment of which requires 11 days when using a lentivirus vector that expresses TuD-miR200c continuously.

INTRODUCTION

MicroRNAs (miRNAs) are small (18–25 nt) non-coding RNAs that suppress the expression of target transcripts at the post-transcriptional level (1–3). There are more than 1500 miRNA species in the human genome (miRBase release 18), and these nucleic acids are now known to play important roles in various biological processes such as stemness, development, differentiation and the cellular defense responses to infection (4–7). As the aberrant high-level expression of certain miRNAs has now often been reported to be associated with cancers and human infectious diseases, analysis of the underlying molecular mechanisms is likely to become much more extensive (8,9). The development of reagents that can strongly suppress specific miRNAs has also generated much interest and will be important for both basic miRNA research and also as a possible therapeutic strategy.

Most synthetic low-molecular weight inhibitors of specific miRNAs are based on anti-miRNA antisense oligonucleotides (AMO), in which some or all of the ribonucleotides are modified to 2′-*O*-methylated RNA (10,11), locked nucleic acids (LNA)/DNA or 2′-methoxyethylated RNA to provide resistance to cellular nucleases and to increase affinity towards complementary miRNA sequences (12,13). In addition, the backbones of some AMOs are substituted with phosphorothioate (14). These modifications and substitutions can be used in combination and some AMOs have flanking sequences or are connected to lipids through the use of linkers (14,15). However, since these reagents will be diluted by successive cell divisions, and in some cases metabolized in the cytoplasm, their effects are transient in many cases. To achieve the long-term suppression of a specific miRNA, specialized plasmid- and virus-vectors carrying expression units for inhibitory RNA molecules have also been developed. These inhibitory RNA molecules include 'antagomir', 'eraser' and 'sponge' (16–18). We have also reported on such plasmid- or lentivirus-based vectors expressing inhibitory RNA targeting specific miRNAs, which we have termed Tough Decoy (TuD) RNA (19).

*To whom correspondence should be addressed. Tel: +81 3 5449 5730; Fax: +81 3 5449 5449; Email: iba@ims.u-tokyo.ac.jp

TuD RNAs have been already used for the basic research, for the identification of miRNA targets (20), and in the functional analysis of miRNA in cancer cells (21), in tumour formation in mice (22) and in myoblast differentiation (23). TuD RNAs are single RNA molecules with a complex secondary structure composed of four elements: a stem of 18 bp in length, two miRNA-binding sites (MBSs) that have a sequence complementary to that of a mature miRNA of interest, a stem–loop structure which connects these two MBSs, four linkers with 3 nt also connecting the two MBSs and flanking stems (Figure 1A). These elements provide efficient nuclear export, binding to the target miRNA, resistance to cellular nucleases and enhancement of the MBS accessibility to the target miRNA, respectively. By screening several alternative MBS sequences to optimize their decoy activity, we have further identified a highly potent TuD, the MBS of which has a 4 nt insertion between positions 10 and 11 from the 3′-end of the perfectly complementary sequence to the entire mature miRNA of interest, where the Ago2-containing RISC cleaves target mRNAs (24). When these TuD RNAs were expressed using lentivirus vectors, they were shown to be efficiently transported to the cytoplasm and exhibit strong inhibitory effects for more than 1 month.

Retro/lentivirus vectors carrying TuD, however, have a potential disadvantage in terms of their therapeutic application as this requires human gene therapy. In our current study, we aimed to develop low-molecular weight reagents that can retain miRNA inhibitory activity even after several rounds of cell division by mimicking the structural features of TuD RNA. We have developed a synthetic miRNA inhibitor composed of two strands of 2′-*O*-methylated RNA oligonucleotides, the structure of which is very similar to that of the corresponding TuD RNA and we have designated this as S-TuD (Synthetic TuD). We provide evidence that if appropriate MBSs are selected, S-TuDs targeting miR-21, -200c, -16 and -106b retain potent inhibitory effects even when transfected at a low dose range of 1 nM–30 pM. We further show that a single transfection of S-TuD-miR200c with the appropriate MBSs can induce a partial epithelial–mesenchymal transition, indicating that the inhibitory effects of S-TuD can withstand dilution by several rounds of cell division.

MATERIALS AND METHODS

MiRNA inhibitors

For the preparation of S-TuD, a series of fully 2′-*O*-methylated RNA oligonucleotide pairs were synthesized as listed in Supplementary Table S1 and each pair was annealed prior to transfection. For the preparation of 5-FAM (Fluorescein-5-carboxamido)-labeled S-TuD, 5-FAM labeled 2′-*O*-methylated RNA oligonucleotide strands were synthesized and annealed with the unlabeled opposite 2′-*O*-methylated RNA oligonucleotide strands (Supplementary Table S1). MiRNA hairpin-inhibitor-miR-21 and miRNA hairpin-inhibitor-miR-106b were purchased from Thermo Scientific (miRIDIAN microRNA Hairpin inhibitors, IH-300492-05 and IH-300649-07, respectively). The anti-miR200c LNA and anti-miR106b LNA antisense oligonucleotide molecules were purchased from Exiqon (miRCURY LNA™ miRNA inhibitors 410126-00 and 426648-00, respectively). Antisense-miR106b was purchased from Life Technologies (AM10067). Technical information regarding the miRNA inhibitors described above is provided in Supplementary Table S2. Anti-miR21 PNA and negative control PNA antisense oligonucleotide molecules were supplied from Panagene (PI-1050 and PN-1001, respectively). Negative control LNA/DNA antisense oligonucleotide was synthesized by GeneDesign. Negative control 2′-*O*-methylated RNA and anti-miR21 2′-*O*-methylated RNA antisense oligonucleotides were synthesized by Hokkaido System Science. The 2′-*O*-methylated RNA AMOs and negative control LNA/DNA AMO sequences are listed in Supplementary Table S3.

Design of the S-TuD negative control sequence

We synthesized a massive number (~1 billion) of random 25 nt RNA sequences *in silico* as candidate negative control molecules. Sequences with GC contents of between 20% and 80% were selected from this panel and were subsequently checked for their complementarity against 735 seed miRNA sequences (second to eighth region from the 5′-end) extracted from the entire human repertoire listed on miRBase Release 14. To exclude sequences which could potentially bind to human endogenous miRNAs, sequences that possessed six or more Watson–Crick type base pairs with any seed sequence were excluded from the list of candidates. A negative control sequence for S-TuD was arbitrarily chosen from a candidate group that had the smallest number of sequences that were complementary to the seed sequences of the entire human miRNA complement.

Plasmid construction

For the construction of luciferase reporter plasmids, the oligonucleotide pairs listed in Supplementary Table S4 were annealed and cloned into the XbaI–FseI sites of pGL4.74 (Promega, Madison, WI, USA) to generate pGL4.74-T21, pGL4.74-T200c, pGL4.74-T16 and pGL4.74-T106b, respectively. For the construction of the h7SK (human 7SK) promoter type TuD shuttle vector, we amplified a 0.3-kb human 7SK promoter fragment by PCR from human genomic DNA using the primers listed in Supplementary Table S5, followed by cloning into pCR2.1 (Invitrogen, Carlsbad, CA, USA). An oligo pair, listed in Supplementary Table S5, was annealed and cloned into this product via KpnI and HindIII sites to generate the ph7SK-TuD-shuttle. For the construction of TuD RNA expression cassettes, a series of oligonucleotide pairs were synthesized (Supplementary Table S6). Each oligo pair was annealed and cloned into the ph7SK-TuD-shuttle at the BsmBI site to generate h7SK-TuD-miR200c and h7SK-TuD-NC cassettes, from which 0.4-kb BamHI–EcoRI fragments were subcloned into the lentivirus vector pLSP to generate pLSP-h7SK-TuD-miR200c and pLSP-h7SK-TuD-NC (19), respectively.

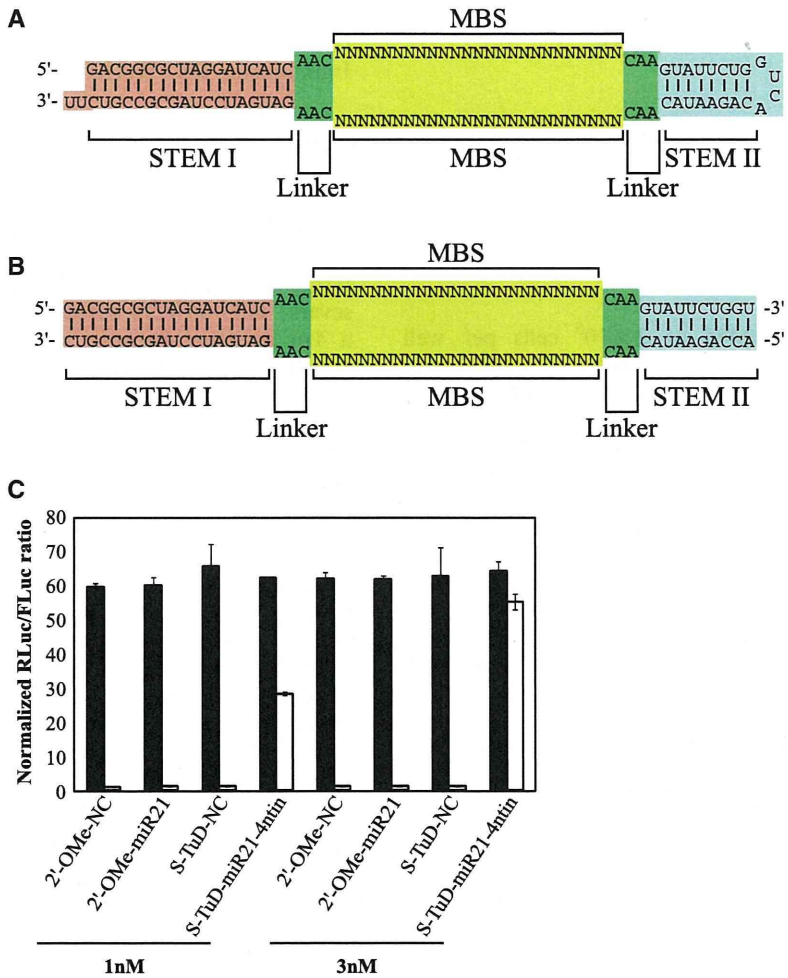

Figure 1. Schematic representation of the structure of S-TuD RNA (**A**) and S-TuD (**B**). (**C**) Inhibitory effects of S-TuD-miR21-4ntin upon endogenous miR-21 activity. S-TuD or 2′-*O*-methylated RNA oligonucleotide-based antisense molecules were transfected into HCT-116 cells together with the *Renilla* luciferase miR-21 reporter (miR-21-RL) (open bars) or the untargeted control *Renilla* luciferase reporter (UT-RL) (black bars) as well as the *Firefly* luciferase reporter (FL) as a transfection control. After performing a dual luciferase assay, the expression levels were normalized to the ratio of the activity of miR-21-RL to that of FL in 1 nM S-TuD-NC transfected HCT-116 cells and are represented by the mean ± SD ($n = 3$).

Cell culture

The human colorectal adenocarcinoma cell line, HCT-116, was obtained from ATCC and cultured at 37°C in DMEM containing 10% fetal bovine serum (FBS).

RNA preparation and quantitative RT–PCR for mRNA

HCT-116 cells were seeded at 1×10^5 cells per well in six-well culture plates at 1 day prior to transfection. S-TuD-miR21-4ntin (0, 0.3, 1 or 10 nM) was transfected using Lipofectamine 2000 (Invitrogen) in accordance with the manufacturer's instructions. Poly(I)-poly(C) dsRNA (100 ng/ml, Sigma) was transfected as a positive control to induce interferon responses. Total RNA was prepared from HCT-116 cells just prior to transfection (0 h) and at 7 and 24 h after transfection using RNeasy (Qiagen). First strand cDNA was then synthesized using a Super Script VILO cDNA synthesis kit (Invitrogen). Real-time RT–PCR was performed using the 7900 HT fast real-time PCR system (Applied Biosystems) with SYBR Green as a reporter. The data were normalized using GAPDH expression, and the levels expressed relative to the pre-transfected conditions (0 h). The sequences of the primers used for real-time PCR are listed in Supplementary Table S7.

Transfection and Luciferase assays

Cells were seeded at densities of 1×10^5 cells per well in 24-well plates in DMEM containing 10% FBS the day before transfection. The cells were then transfected in triplicate with Lipofectamine 2000 and 10 ng of *Firefly* luciferase plasmid pTK4.12 (Supplementary Figure S1A), 100 ng of RLuc target reporter plasmid and various concentrations of miRNA inhibitors (0.003 and 25 nM; Supplementary Figure S1B–S1F). We performed

all assays at 48 h after the transfection using the dual luciferase assay on Glomax (Promega).

UV spectroscopy

Each S-TuD was dissolved in 10 mM sodium phosphate (pH 7.0) containing 10 mM NaCl. The UV-melting curves of 1.5 μM S-TuD at 260 nm were measured on a Shimazu UV-2450 UV–VIS spectrophotometer with a melting rate of 0.5°C/min.

MiR qRT–PCR

HCT-116 cells were seeded at 2×10^5 cells per well (six-well plates) in DMEM containing 10% FBS and transfected with 0.05 nM of S-TuD-miR106b-pf using the siPORT NeoFX transfection reagent (Ambion) according to the manufacturer's instructions. Total RNA was prepared from HCT-116 cells at 48 h after transfection using mirVana miRNA Isolation Kit (Applied Biosystems, CA, USA). Expression of mature miRNAs was determined by miR-qRT–PCR using miRNA-specific looped RT-primers and TaqMan probes as recommended by the manufacturer (Applied Biosystems). U6 snRNA was used as an internal control. PCR was performed in triplicate using the 7300 Real-Time PCR System (Applied Biosystems).

Oligonucleotides transfection, FACS analysis and sorting

HCT-116 cells were seeded at 2×10^5 cells per well (six-well plates) in DMEM containing 10% FBS and transfected with 10 nM of 5-FAM-labeled S-TuD-miR200c-pf or S-TuD-NC using the siPORT NeoFX transfection reagent (Ambion). To specifically isolate miRNA inhibitor-transfected cells, 5-FAM positive cells were sorted using FACS Aria (BD).

Virus transduction and Luciferase assays

HCT-116 cells were seeded at 1×10^5 cells per well in six-well plates in DMEM containing 10% FBS. After 24 h, the cells were transduced with each TuD RNA virus stock (3×10^5 TU) in the presence of 8 μg/ml of polybrene. After a further 24 h, the medium was then substituted with DMEM containing 10% FBS and puromycin (1 μg/ml). After 7 days of selection, the puromycin was removed from the medium.

Western blotting

Total proteins were extracted from cells using 1.5× SDS denaturing buffer and protein concentrations were measured using the Bio-Rad protein assay kit. The protein extracts were separated by 12% SDS–PAGE and transferred onto a PVDF membrane (Millipore). Immunoblotting was performed by incubating the membrane with antibodies against E-cadherin (ab76055, Abcam), vimentin (sc-6260, Santa Cruz), ZEB1 (ab64098, Abcam) and actin (612656, BD transduction) for 2 h at room temperature. Secondary antibodies conjugated with horseradish peroxidase were incubated with the membranes for 1 h at RT after three washes with phosphate-buffered saline with Tween-20. Signals were detected on an imaging analyzer LAS4000-EPUVm (FUJIFILM) using ECL reagent (Amersham) or Immunostar DL (WAKO).

RESULTS

Synthesis of two modified RNA strands that form a structure resembling TuD-miR21-4ntin after hybridization

We have previously reported the design of TuD RNAs targeting miR-21, miR-140 and miR-16. Among the several TuD-miR21s constructed, TuD-miR21 harboring a 4 nt insertion between positions 10 and 11 from the 3′-end of the perfectly complementary sequence to miR-21, where the RISC cleaves the target mRNAs (TuD-miR21-4ntin), exhibited the most potent inhibitory effects when expressed from a plasmid vector. A potential approach to the development of other potent TuDs was therefore to synthesize 2′-*O*-methylated RNA oligonucleotides that have the same sequence as TuD-miR21-4ntin. However, the synthesis of the full length molecule of TuD-miR21-4ntin (122 nt) in large amounts would not have been easy using current techniques. Considering also that the both sides of the two MBS sequences in a TuD molecule are flanked by two dsRNA stems, we decided to separate the entire TuD-miR21-4ntin molecule into two strands (60 nt each) by cutting the middle of the loop region so that the structure formed after the hybridization of both strands resembled that of TuD-miR21-4ntin (Figure 1B).

To test whether such hybridized 2′-*O*-methylated RNA strands would suppress endogenous miR-21 activity in HCT-116 cells (which express very high levels of endogenous miR-21), we transiently cotransfected them with dual luciferase reporters (DLR), which are composed of the *Renilla* luciferase reporter with or without the insertion of a 22-bp DNA sequence fully complementary to the mature miR-21 within the 3′-UTR (Supplementary Figure S1BC). The firefly luciferase reporter was used as a transfection control (Supplementary Figure S1A). As shown in Figure 1C, the hybridized 2′-*O*-methylated RNA inhibited endogenous miR-21 activity much more efficiently than the conventional 2′-*O*-methylated RNA oligonucleotide AMO, when 1–3 nM of these inhibitors were introduced. Appreciable inhibitory effects of the AMO, 2′-*O*-methylated RNA and PNA oligonucleotide, were only observed at a concentration of 50 nM (Supplementary Figure S2). We designated this 2′-*O*-methylated RNA-based inhibitor of miRNA with a similar structure to TuD as S-TuD (synthesized TuD) and decided to further optimize its inhibitory effects.

Since S-TuD harbors two regions with a complete double stranded structure (18 and 10 bp, respectively), we speculated that it might potentially trigger an interferon response in the introduced cells and thus disrupt any functional analysis of miRNAs. To test this possibility, we transfected HCT-116 cells with S-TuD-miR21-4ntin as well as Poly I:C as a positive control and the mRNA levels of the interferon responsive genes *OAS1*, *OAS2*, *MX1*, *IRF9* and *IFITM1* were determined at 0–24 h after transfection by quantitative RT–PCR

(Figure 2). The results clearly showed that S-TuD does not induce an immune response in cell cultures even at the highest concentration used (10 nM) as judged by the interferon induction level. Essentially similar results were obtained when DLD-1 cells were used (data not shown).

Modulation of the MBS sequence of S-TuD to obtain optimum inhibitory effects

TuD-miR21-4ntin has two MBS regions which carry a 4 nt-insertion between positions 10 and 11 from the 3′-end of the perfectly complementary sequence to mature miR-21, where the RISCs cleave the target mRNAs. This insertion sequence is designed to form a 4-nt bulge when the target miRNA binds to the MBS of the corresponding TuD. Through the presence of this bulge, we previously demonstrated that TuD-miR21-4ntin efficiently escapes from this cleavage and has a much higher inhibitory effect than TuD-miR21-pf (TuD-miR21 harboring MBSs perfectly complementary to miR-21). Since S-TuD is composed of fully 2′-*O*-methylated RNA, we tested whether it would require this 4-nt insertion to avoid cleavage. We compared the inhibitory effects of S-TuD carrying MBSs with or without the 4-nt bulge, using S-TuDs targeting miR-21 and miR-200 c, respectively. Whereas S-TuD-miR21-4ntin inhibited miR-21 more efficiently than S-TuD-miR21-pf at the same dosage (Figure 3A), the inhibitory effects of 0.1 nM S-TuD-miR200c-pf were even greater than those exerted by 0.3 nM S-TuD-miR200c-4ntin (Figure 3B).

To resolve the apparent discrepancies found in the requirement of the bulge for higher S-TuD activity, we next examined the possible secondary structures of these S-TuDs using CentroidFold (http://www.ncrna.org/centroidfold) (25). CentroidFold can predict the secondary structure of a single native RNA molecule but not one composed of two strands of 2′-*O*-methylated RNAs. We therefore analyzed the TuD RNA that has the same MBS sequences as the corresponding S-TuD to obtain an approximate secondary structure (Supplementary Figure S3). When the base pair formation between the two MBSs in the S-TuD targeting miR-21 was compared, it was much stronger in S-TuD-miR21-pf than in S-TuD-miR21-4ntin. On the other hand, the interaction between the two MBSs of S-TuD-miR200c-4ntin was found to be higher than that of S-TuD-miR200c-pf. From these observations, we speculated that the accessibility to the target miRNA drastically decreases if the interaction between the two MBSs of one S-TuD molecule is very strong. To test this hypothesis, we attempted to introduce a point mutation in MBSs, which would reduce the heavy base pair formation between the two MBSs of S-TuD-miR21-pf without significantly affecting the binding activity. Regions close to the 5′- and 3′-ends of the MBS would then not easily form base pairs because the linkers that flank these regions were designed not to hybridize to each other. Point mutations at any positions complementary to the seed regions or the 3′-compensatory sites would also drastically reduce the miRNA inhibitory effects and point mutations at any positions complementary to the seed regions would affect

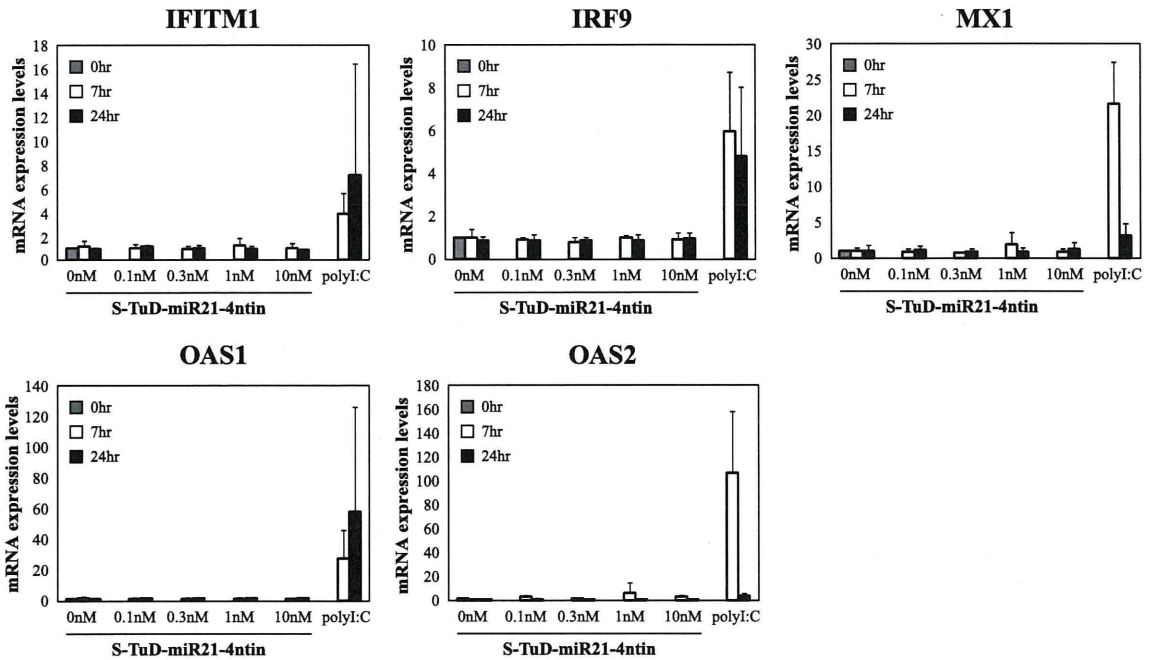

Figure 2. Measurement of the interferon response in cells transfected with S-TuD. S-TuD-miR21-4ntin was transfected into HCT-116 cells at several doses. Interferon response genes were then measured by qRT–PCR and are represented by the mean ± SD ($n = 3$). Poly(I)-poly(C) dsRNA (100 ng/ml) was used as a positive control.

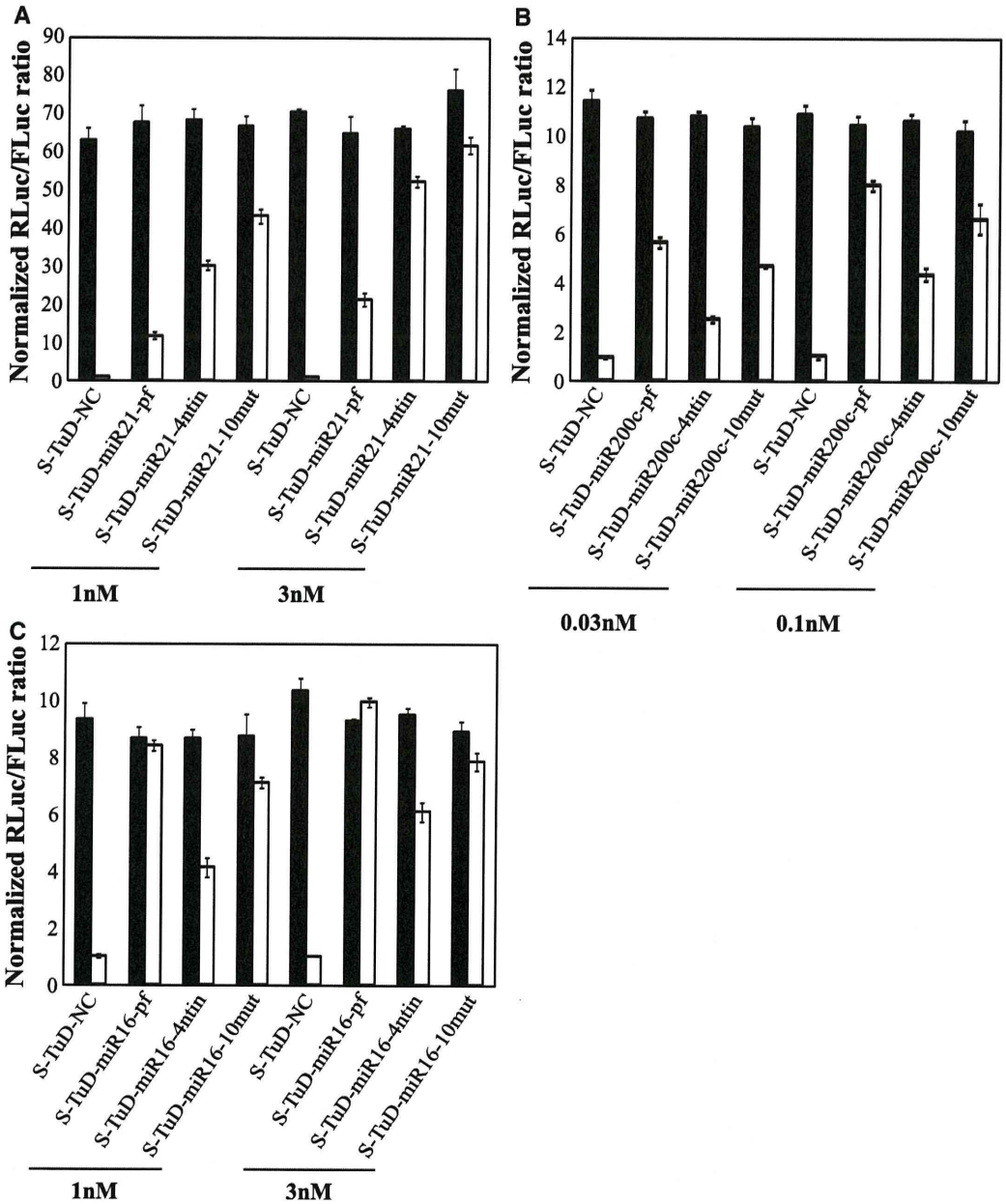

Figure 3. Impact of MBS sequences on the inhibitory effects of S-TuD molecules. (**A**) Comparison of three types of S-TuD-miR21 (S-TuD-miR21-pf, S-TuD-miR21-4ntin, and S-TuD-miR21-10mut). HCT-116 cells were transfected using similar procedures to those shown in Figure 1C. After performing a dual luciferase assay, the expression levels were normalized to the ratio of the activity of miR-21-RL to that of FL in 1 nM S-TuD-NC transfected HCT-116 cells and are represented by the mean ± SD (n = 3). (**B**) Comparison of three types of S-TuD-miR200c (S-TuD-miR200c-pf, S-TuD-miR200c-4ntin, and S-TuD-miR200c-10mut) which were transiently transfected into HCT-116 cells together with the *Renilla* luciferase miR-200 c reporter (miR-200 c-RL; open bars) or the untargeted control *Renilla* luciferase reporter (UT-RL; black bars). In all cases, the *Firefly* luciferase reporter (FL) was cotransfected as a transfection control. After performing a dual luciferase assay, the expression levels were normalized to the ratio of the activity of miR-200c-RL to that of FL in 0.03 nM S-TuD-NC transfected HCT-116 cells and are represented by the mean ± SD (n = 3). (**C**) Comparison of three types of S-TuD-miR16 (S-TuD-miR16-pf, S-TuD-miR16-4ntin, and S-TuD-miR16-10mut) which were transiently transfected into HCT-116 cells together with the *Renilla* luciferase miR-16 reporter (miR-16-RL; open bars) or the untargeted control *Renilla* luciferase reporter (UT-RL; black bars). In each case, the *Firefly* luciferase reporter (FL) was cotransfected as a transfection control. Following a dual luciferase assay, the expression levels were normalized to the ratio of the activity of miR-16-RL to that of FL in 1 nM S-TuD-NC transfected HCT-116 cells and are represented by the mean ± SD (n = 3).